BASE DRAG REDUCTION BY EXTERNAL BURNING

Gary Joe Caswell

NAVAL POSTGRADUATE SCHOOL
Monterey, California

THESIS

BASE DRAG REDUCTION BY

EXTERNAL BURNING

by

Gary Joe Caswell

Thesis Advisor: A. E. Fuhs

September 1973

Approved for public release; distribution unlimited.

Base Drag Reduction by External Burning

by

Gary Joe Caswell
Lieutenant junior grade, United States Navy
B.S., University of Colorado, 1969

Submitted in partial fulfillment of the
requirements for the degree of

MASTER OF SCIENCE IN AERONAUTICAL ENGINEERING

from the

NAVAL POSTGRADUATE SCHOOL
September 1973

ABSTRACT

Supersonic combustion in the inviscid stream has been shown to reduce the base drag on a projectile. Fast reacting fuel burned externally in the inviscid, supersonic flow generates compression waves, which, when properly originated, impinge on the recirculation bubble aft of the projectile base and increase the base pressure. A free-jet wind tunnel was constructed to study external burning where heat addition was simulated by nozzle contour. Sufficient increase in base pressure was attained to not only reduce base drag but also provide thrust. Thus, external burning provides a method for increasing the performance of projectiles.

TABLE OF CONTENTS

LIST OF TABLES

LIST OF FIGURES

LIST OF SYMBOLS

English

a = limiting angle shown in Fig. 2

a_t = speed of sound

A = area

A_B = base area

A_h = area of heat addition zone in Fig. 15

A_e = area of isentropic stream in Fig. 15

b = capture height of heat addition zone

C_{PB} = coefficient of base pressure

d = wake diameter

D_B = base drag

F_B = force on the base

$g(x)$ = function defined in Eq. (6)

h = base half height

Δh_f = heat release per unit mass of fuel

I_{sp} = specific impulse

l = distance from base corner to first fully developed compression wave

L = finite body length

M_∞ = Mach number at infinity

$M_l = M_b$ = Mach number ahead of base corner

M_e = Mach number in isentropic stream

$\dot{m}_f$ = fuel flow rate

P = pressure

P_∞ = pressure at infinity

P_B = pressure on the base

P_b = pressure ahead of base corner

P_e = pressure in isentropic stream

q = heat release per unit volume per unit time

r = body radius

Re = Reynolds number

T_B = base temperature

$u = v$ = flow velocity

$\Delta V/V$ = constant pressure volume expansion

W = length of heat addition zone

W_e = ratio of x component of velocity to the speed of sound = u_x/a_z

X_i = axial distance to start of combustion as shown in Fig. 13

Y_i = radial distance to start of combustion as shown in Fig. 13

Greek

β = body angle shown in Fig. 4

β_B = $\sqrt{M_B^2-1}$

γ = C_p/C_v = ratio of constant pressure specific heat to constant volume specific heat

δ = boundary layer thickness

δ^* = displacement thickness

δ^{**} = momentum thickness

η = a heating parameter defined in Eq. (8)

θ = angle of inclination of heat addition zone in Fig. 4

μ = air to fuel ratio

μ_∞ = free stream air viscosity

ν = Prandtl Meyer angle/function

ρ = air density

ϕ = perturbation velocity potential

ω = angular velocity

ACKNOWLEDGEMENTS

The author wishes to thank Professor A. E. Fuhs for his guidance and support as thesis advisor. The author also would like to express his thanks to CDR Smithey for his work on the same subject and to Messrs. H. Conners and J. Moulton for their technical assistance. Finally, the author wishes to express appreciation to Mr. Dominic Monetta and Dr. Alan Roberts of Gun Systems Engineering, Naval Ordnance Station, Indian Head, Maryland, for their support.

I. INTRODUCTION

For an axisymmetric object flying at supersonic speed as much as 50 percent of the overall drag can be attributed to the negative gage pressure acting upon the base. This relationship between base drag and the remaining drag on the body, which consists of wave, skin friction, and boat-tail drags, is observed primarily in the low supersonic flight regime. For Mach numbers near 2 the pressure on the base can be reduced to as little as 50 percent that of the ambient air while the nose pressure can be kept relatively low by using slender, streamlined shapes. With increasing Mach number, however, a limit to the base drag is reached since the base pressure cannot be less than a negative one atmosphere, whereas the pressure on the nose will continue to increase with Mach number.

The reduction of drag is desirable in order to increase the range and terminal velocity of a projectile. Pressure or wave drag and skin friction drag have been satisfactorily reduced by designing streamlined shapes. Base drag, however, has not been reduced significantly although the use of boat-tails and base bleed have contributed slightly. The most promising method of base drag alleviation is that due to external burning. Heat addition in the inviscid flow in proximity of the base will create compression waves that, if optimally originated, will impinge on the base flow region. The interaction of these compression waves will

deflect the free streamline toward the symmetric axis, and the static pressure in the recirculation zone will increase thus reducing the base drag.

II. THEORY

The base flow problem is visualized most easily with the inviscid flow model in Fig. 1 which ignores the effects of viscosity.

A. INVISCID FLOW

A semi-infinite, two-dimensional model can be formulated which easily satisfies all the necessary boundary conditions.

1. Two-Dimensional Model

If a value of P_B (= base pressure) is selected, then the initial turning through the Prandtl Meyer expansion is uniquely determined. The pressure and, therefore, the

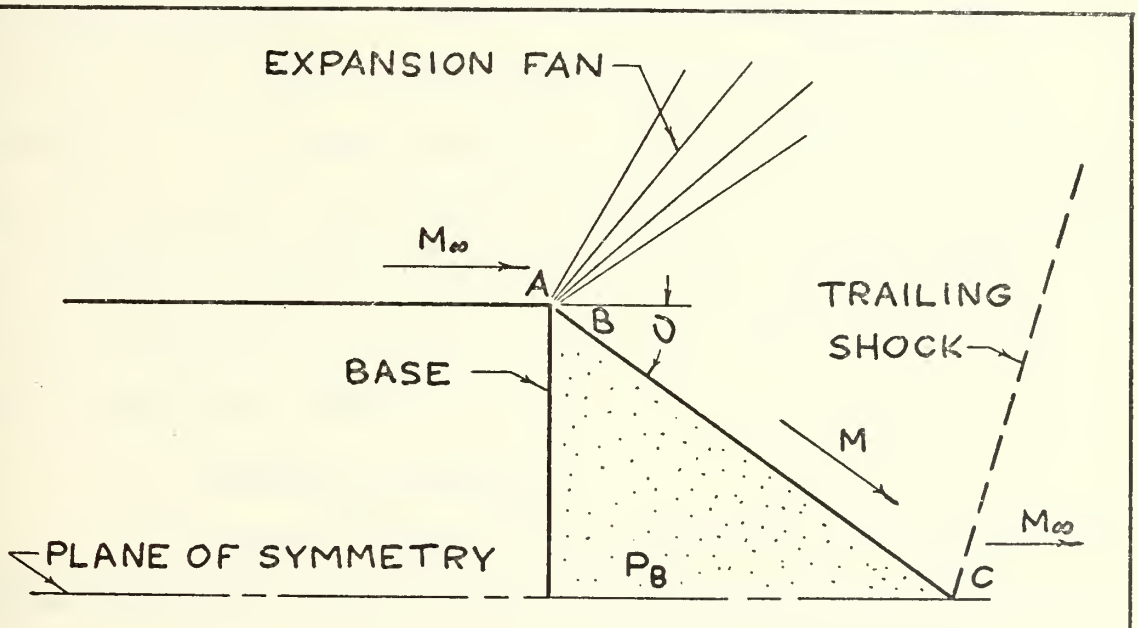

FIG. 1
TWO-DIMENSIONAL INVISCID FLOW

velocity and Mach number are constant along the streamline BC. The Mach number can be calculated from the Prandtl Meyer equations. For uniform, two-dimensional flow over a convex corner, the pressure depends only on the angle of inclination of the free streamline (angle θ in Fig. 1), and thus BC is a straight line. The shock wave originating at C is weakened eventually by the interaction of the expansion waves. Near the plane of symmetry, the shock must return the flow to the free stream direction. As the flow continues downstream of the trailing shock, the static pressure approaches the free stream pressure. Unfortunately, for a given M_∞, an infinite number of possible solutions exist. As P_B is decreased, the Prandtl Meyer angle is increased, and point C moves closer to the base. A limit is reached eventually where for a given local Mach number M_1, the trailing shock cannot return the flow to its original direction. The maximum deflection shock wave for a given local Mach number determines a limiting flow from the infinite number of possible solutions. This limiting case yields the minimum possible P_B and thus the maximum base drag in inviscid flow.

2. Axisymmetric Model

Inviscid theory can be extended to axisymmetric shapes with some complications. The expansion characteristics issuing from the base corner are not straight lines as in the Prandtl Meyer flow except near the corner. Because the flow conditions upstream of the trailing shock are dependent not only on the streamline inclination at the

base corner but also on the history of the flow upstream of the Mach lines passing through the corner, the free streamline of constant pressure is not straight, as shown in Fig. 2. The method of characteristics can be utilized in order to determine possible flow patterns.

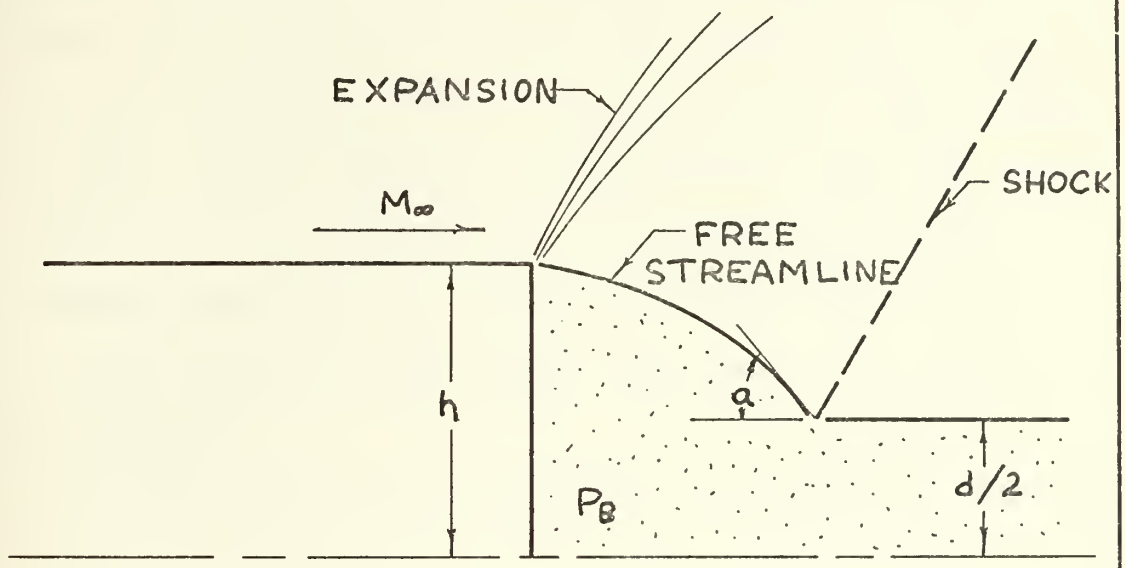

FIG. 2

AXISYMMETRIC INVISCID FLOW

The inviscid flow pattern of an axisymmetric body cannot be constructed to the axis of symmetry and still satisfy the boundary conditions. This is a consequence of the curvature of the free streamline and the fact that for a given Mach number, a single trailing shock is limited in the amount of

turning it can provide. The angle of inclination of the constant pressure free streamline continues to increase monotonically as the axis of symmetry is approached. The flow pattern, therefore, cannot be continued beyond a point where the limiting angle (a in Fig. 2) exceeds the angle that the single trailing shock wave can return the flow parallel to the axis. In real flows, the wake prevents the free streamline from reaching the axis, and thus this limitation yields some similarity to observed flows. Flow fields containing a free streamline which does not reach the axis of symmetry can be considered as those that would exist in an inviscid flow about an axisymmetric body which has an infinitely long cylindrical sting attached at the base as shown in Fig. 3.

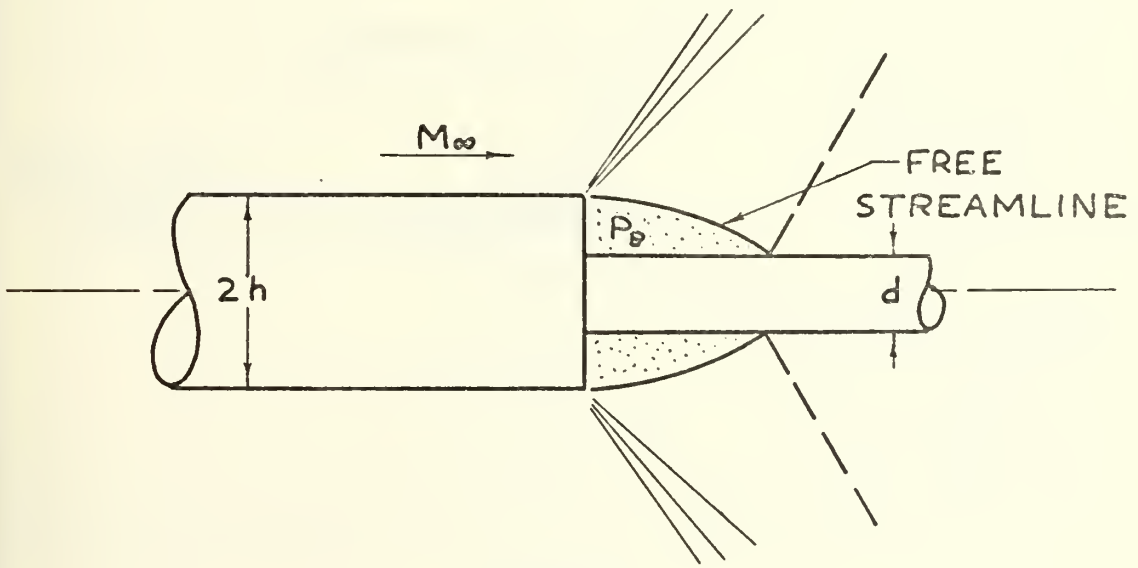

FIG. 3
CHAPMAN ANALOGY BETWEEN WAKE DIAMETER AND INVISCID FLOW ROD DIAMETER

The fraction d/2h equals the ratio of rod diameter to body diameter. As d/2h approaches one, the two-dimensional result for P_B is obtained. With a rod present, inviscid theory predicts a lower base pressure and consequently a higher base drag for two-dimensional profiles than for axisymmetric shapes.

This is in qualitative agreement with the experiment. Chapman [Ref. 1] found that the base drag of axisymmetric bodies in an inviscid flow was so small that it could not account for observed drag values determined from experiment in real fluid flow. This strongly suggested that viscous effects were essential in determining base flow.

B. VISCOUS FLOW

The inclusion of viscosity effects results in a more complicated flow model as shown in Fig. 4. The fluid viscosity

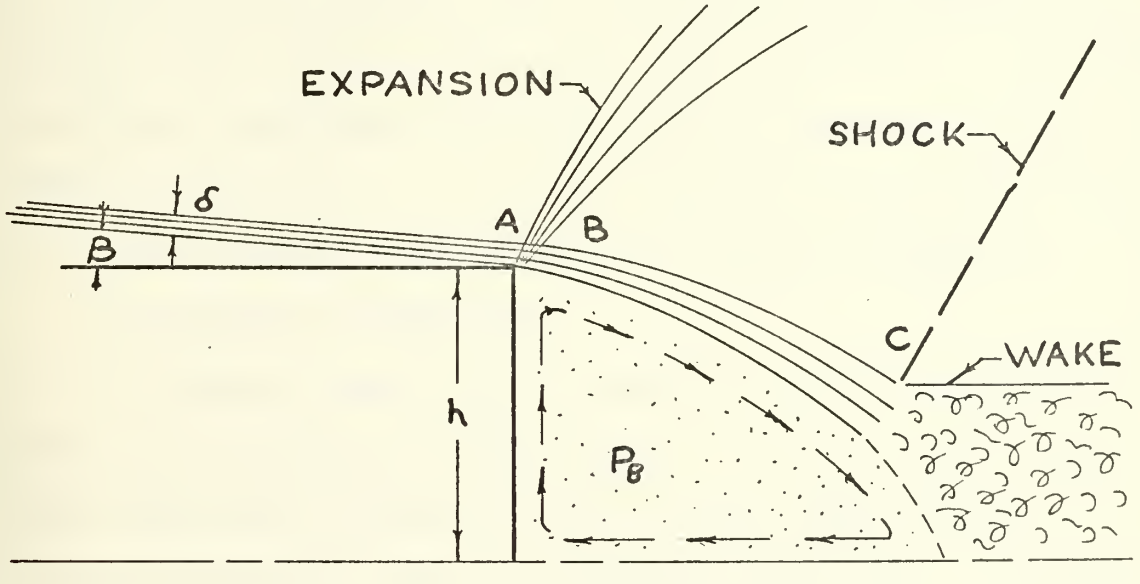

FIG. 4
VISCOUS FLOW AT THE BASE

causes a slow circulatory motion in the dead air region, and the viscous mixing process causes the boundary layer to thicken as it approaches the trailing shock wave. The base pressure arrives at a steady state equilibrium value because of the scavenging effect of the outside flow on the recirculation region. As some of the dead air mass is removed, the angle of turning at the base corner is increased, and consequently the base pressure is decreased. The larger turning angle increases the flow velocity outside the boundary layer which increases the scavenging action, thereby lowering the base pressure. The process is repeated until point C in Fig. 4 reaches an equilibrium position. As point C moves toward the base, however, the pressure ratio of the trailing shock wave increases, making it more difficult for the scavenged air and the low velocity air in the boundary layer to overcome the pressure rise. An equilibrium position is reached which balances these two opposing effects. Viscosity, therefore, determines a unique solution from the infinite number possible for a given Mach number and Reynolds number but, unfortunately, complicates the theory excessively.

C. CHAPMAN'S CORRELATION

Viscous theory is too involved to be a practical method for estimating base pressure. Instead many correlations have been attempted to aid in the understanding or to create a practical means of predicting base drag. According to Chapman's model [Ref. 1] base pressure depends on the Mach number and pressure at the base corner, the boundary layer thickness δ, the body diameter 2h, and the body angle

β at the base. For finite bodies, as shown in Fig. 5, profile shape directly affects the Mach number and pressure at the base corner since the existence of a bow shock wave, for example, would alter the Mach number and pressure prior to the corner.

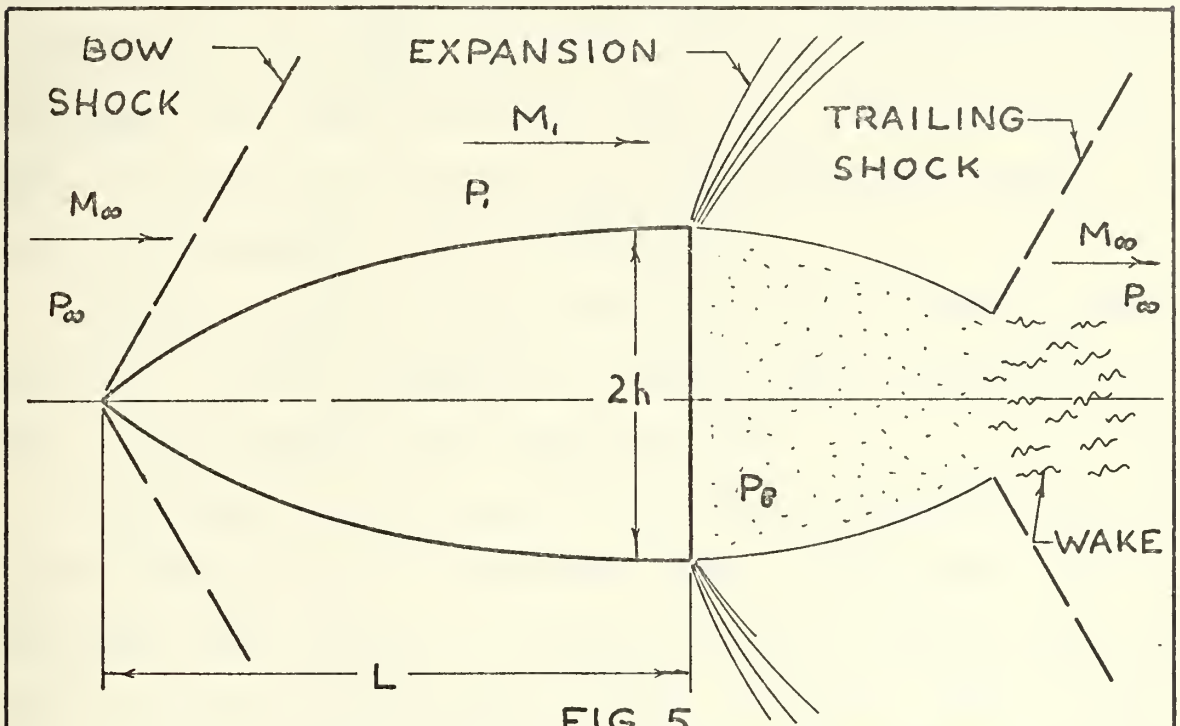

FIG. 5
FINITE BODY EFFECTS

M_1 and P_1 are needed instead of M_∞ and P_∞. Chapman offered a simple means of calculating the corrected approach Mach number M_1 and pressure P_1. He suggested extending the after body one diameter (2h) and taking the average Mach number and pressure along this extension as the corrected M_1 and P_1. From dimensional analysis, Chapman found that $C_{pB} = F(M_1, \delta/h, \beta)$ where C_{pB} is the base pressure coefficient and is equal to $(P_B - P_1)/(\rho_1 V_1^2/2)$. Viscous effects

were included in a Reynolds number dependency of the boundary layer thickness δ. Reynolds number, $Re = \rho_\infty V_\infty L/\mu_\infty$, is based upon the finite body length L and the free stream conditions. ρ_∞ is the free stream air density, V_∞ is the velocity, and μ_∞ is the coefficient of viscosity. Assuming a fixed M_∞, boundary layer theory predicts boundary layer thickness δ is proportional to $1/\sqrt{Re}$ for laminar flow or δ is proportional to $1/(Re)^{1/5}$ for turbulent flow. With $\beta = 0$, the final result from dimensional analysis is $C_{pB} = f(L/hRe^{1/2})$ for laminar flow and $C_{pB} = f(L/hRe^{1/5})$ for turbulent flow.

Chapman used data from axisymmetric flow to make a correlation of C_{pB} with $L/hRe^{1/2}$ for laminar flow, as shown in Fig. 6, and $L/hRe^{1/5}$) for turbulent flow.

The effect of both Re and body shape is apparent, and the laminar correlation is reasonably close to the data. For turbulent flow, Chapman's correlation again is good; however, Re has a much smaller effect on base pressure. This is consistent with theoretical considerations since $1/Re^{1/5}$ is much less Re dependent than is $1/Re^{1/2}$.

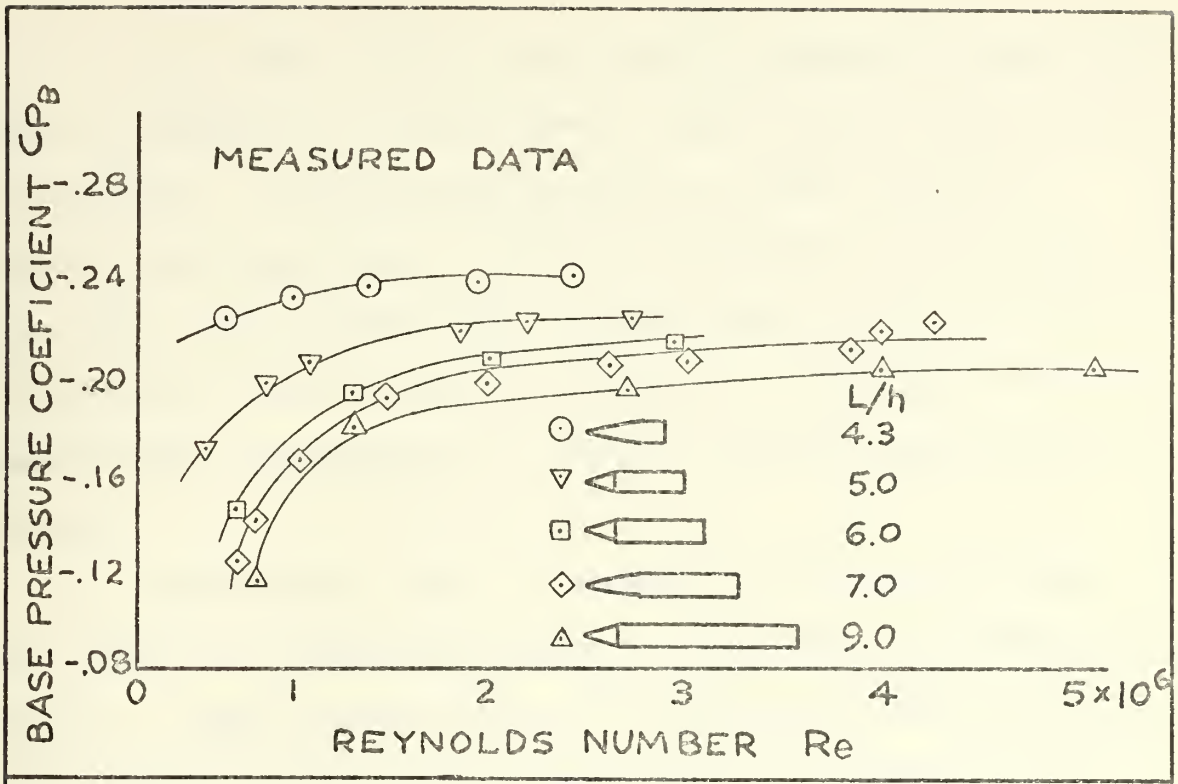

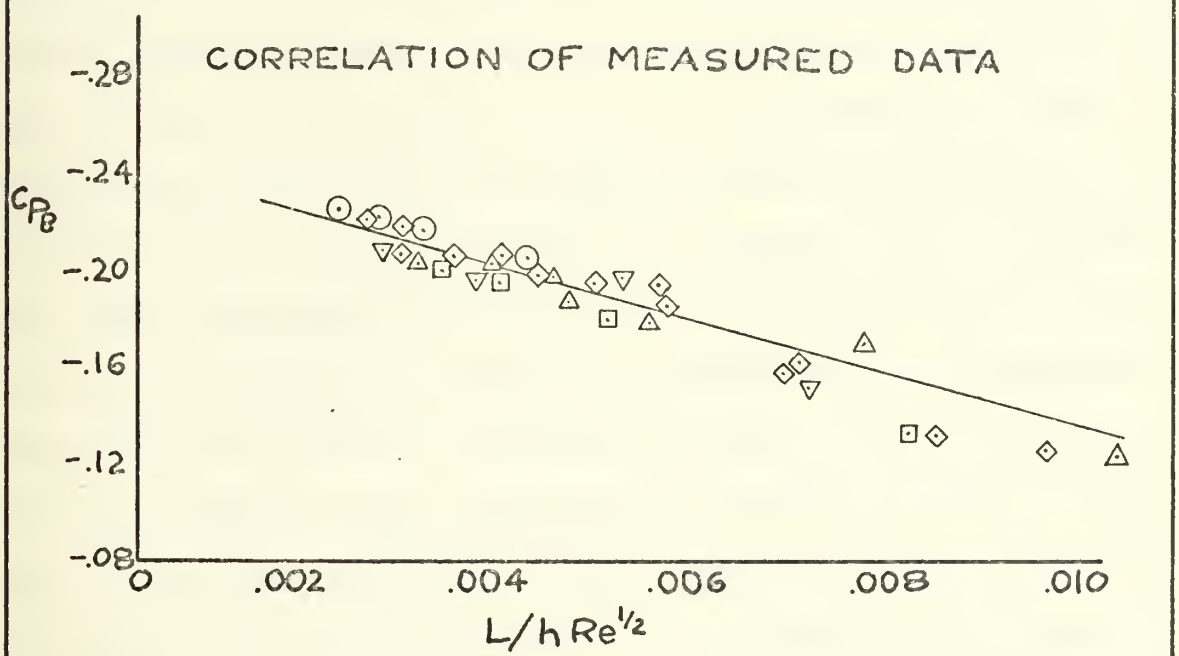

FIG. 6
MEASURED AND CORRELATED BASE PRESSURE DATA FOR M_∞=1.53 LAMINAR BOUNDARY LAYER FLOW
REF. 1

D. EFFECTS OF SPIN

The effect of spin, or a body's revolution about its axis of symmetry, on base pressure also has been shown to be considerable. Unclassified material on this subject is lacking, and apparently no purely theoretical approach has ever been made successfully. It has been concluded instead of analysis, that in order to determine the effects of spin, experimental measurements on specific object shapes need to be made.

C. Wieselsberger [Ref. 9] showed in 1927 that the drag coefficient of bodies at subsonic speeds could be increased by spin. Based on drag data of a projectile and cylinder at low subsonic speeds with circumferential velocities up to three times the forward velocity, Wieselsberger concluded that the increase of total drag resulted from increases in skin friction and base drag due to spin induced alterations of the boundary layer velocity profile. R. Lehnert [Ref. 9] showed that spin influenced the aerodynamic characteristics of projectiles at supersonic speeds, but comprehensive information concerning the effect of spin was lacking. H. H. Kurzweg [Ref. 7] showed a close relationship between boundary layer and base pressure, as did Chapman, which prompted a study by R. Lehnert and S. Hastings [Ref. 9] to determine the base pressure behavior as a functional of spin rate. Experiments were conducted at the Naval Ordnance Laboratory in a supersonic aeroballistics tunnel. Cone cylinders of varying lengths were spun at rates varying from 0 to 43,000 rpm, and base pressure was measured through an orifice located on the

sting immediately adjacent to the model base. Spark-schlieren photographs were taken in order to study the effect of spin rate upon the wake.

In Fig. 7 base pressure ratio was plotted versus model spin rate with the dimensionless model length as a parameter.

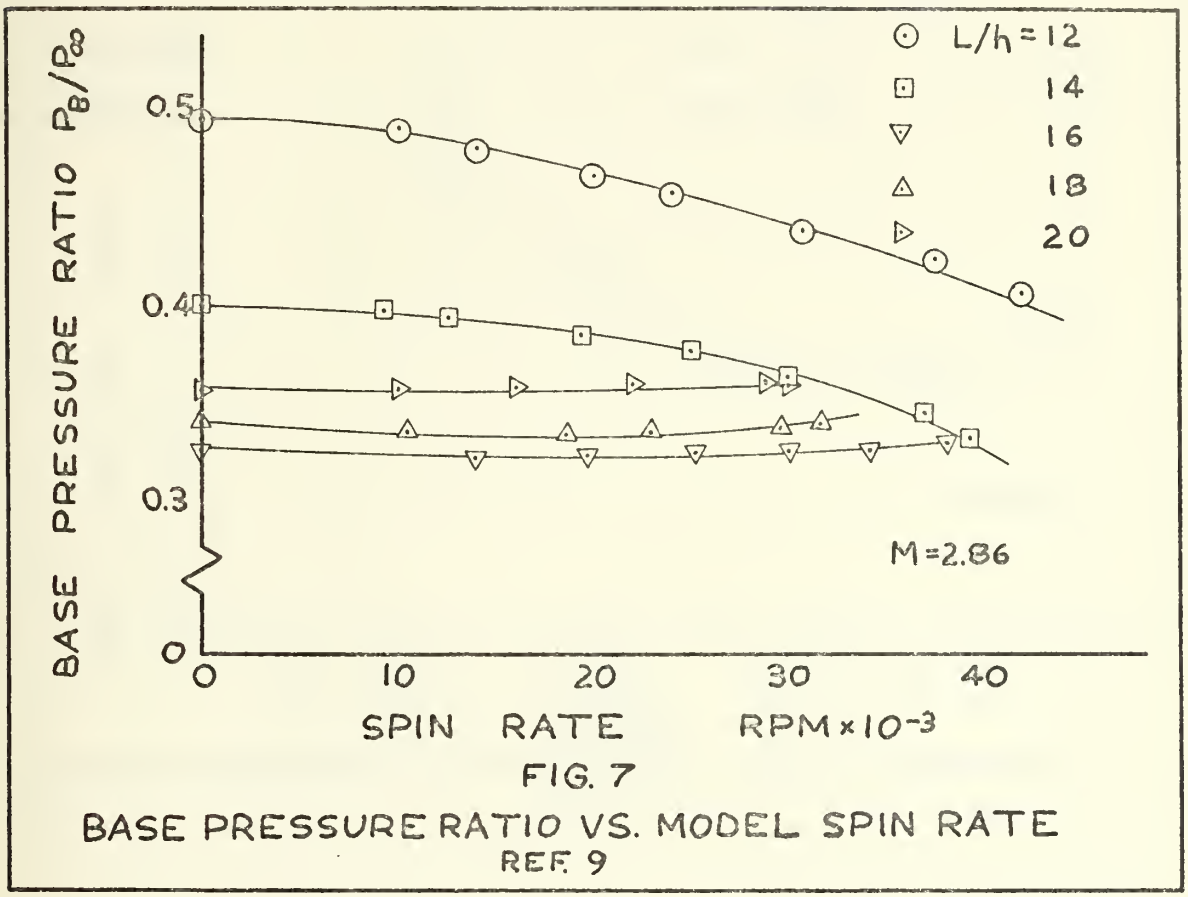

FIG. 7

BASE PRESSURE RATIO VS. MODEL SPIN RATE

REF 9

The upper curve, which corresponds to the shortest model, shows a considerable decrease in base pressure ratio with increasing spin rate. The next lower curve also shows a decrease in P_B/P_∞ with increasing spin rate. The three lower curves, corresponding to the three longest models, show relatively little change in the base pressure ratio with changing spin rates. As was determined by both Kurzweg and Chapman, for a given Mach number and model configuration, the shape of the

curve for base pressure versus Reynolds number is determined by the state of the boundary layer.

Figure 8 shows base pressure ratio plotted against Reynolds number for Lehnert and Hastings' data.

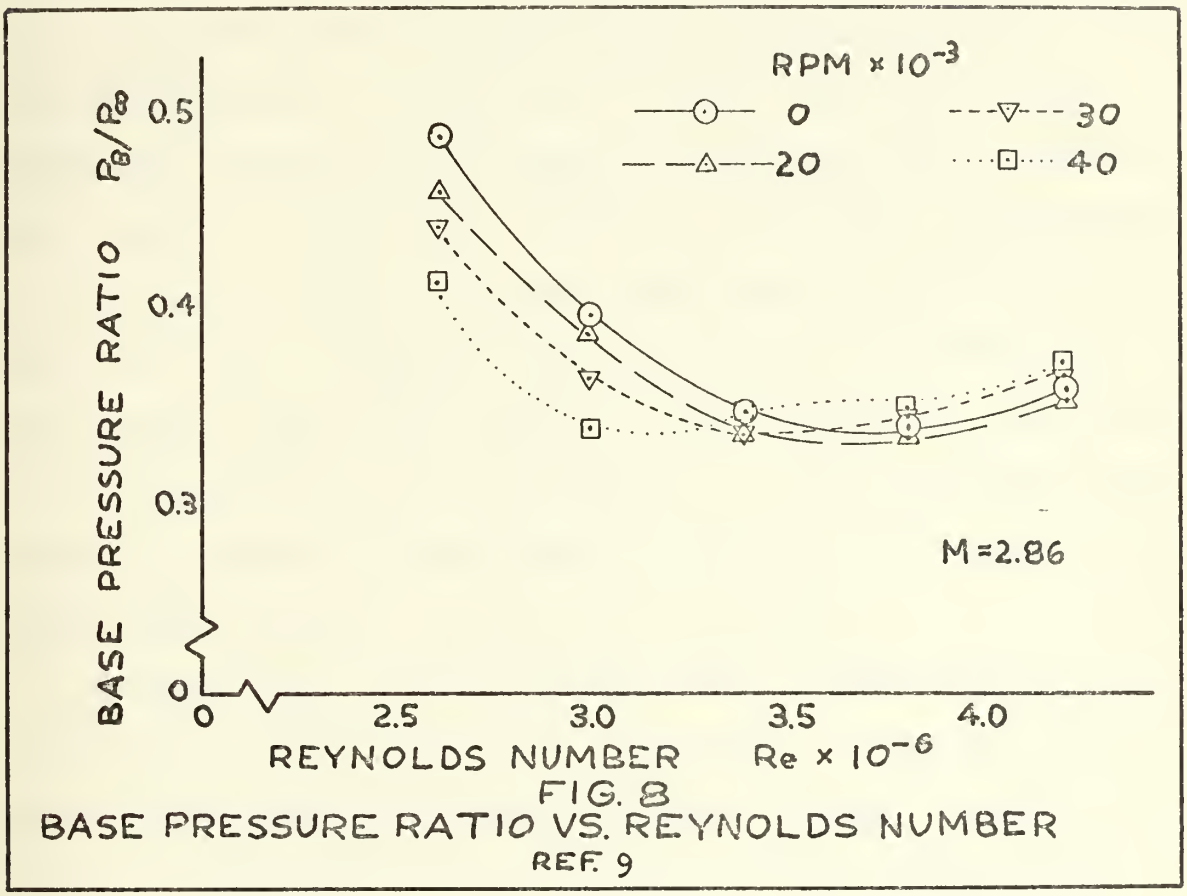

FIG. 8
BASE PRESSURE RATIO VS. REYNOLDS NUMBER
REF. 9

The Reynolds number was referred to free stream conditions and the wetted model length. The first curve shows the zero spin data. The large decrease in P_B with increasing Re up to 3.6 million is accompanied by the existence of a laminar boundary layer along the entire model length. Further increases in Re resulted in a decrease in P_B, and the transition in the wake mixing zone appeared to move upstream. Base pressure reached its minimum value when transition occurred at the model base and increased only slightly at higher Re

when transition occurred upstream of the base. The curves for various spin rates show a considerable decrease in base pressure with increased spin when laminar flow existed at the base. This decrease in base pressure due to spin was accompanied by an upstream travel of transition in the mixing zone as was the case for zero spin. In the transition region, the base pressure is unaffected by spin when the boundary layer is turbulent at the base. Increasing spin resulted in a slight base pressure increase. The minima of the base pressure versus Re curves move toward lower Re with increasing spin rate. It can be concluded that spin destabilizes the boundary layer and thereby produces premature transition. Transition at zero spin was observed to occur at nearly one diameter upstream of the base while at 40,000 rpm, the transition moved to almost two diameters upstream.

Kurzweg [Ref. 8] and Chapman [Ref. 1] observed that base pressure and wake length were correlated. Decreasing base pressure corresponds to decreasing wake length as shown in Fig. 9. This was confirmed by Lehnert and Hastings [Ref. 9] and suggested a method of measuring base pressure on free flight projectiles. Note the similarities of Fig. 9 with Fig. 7.

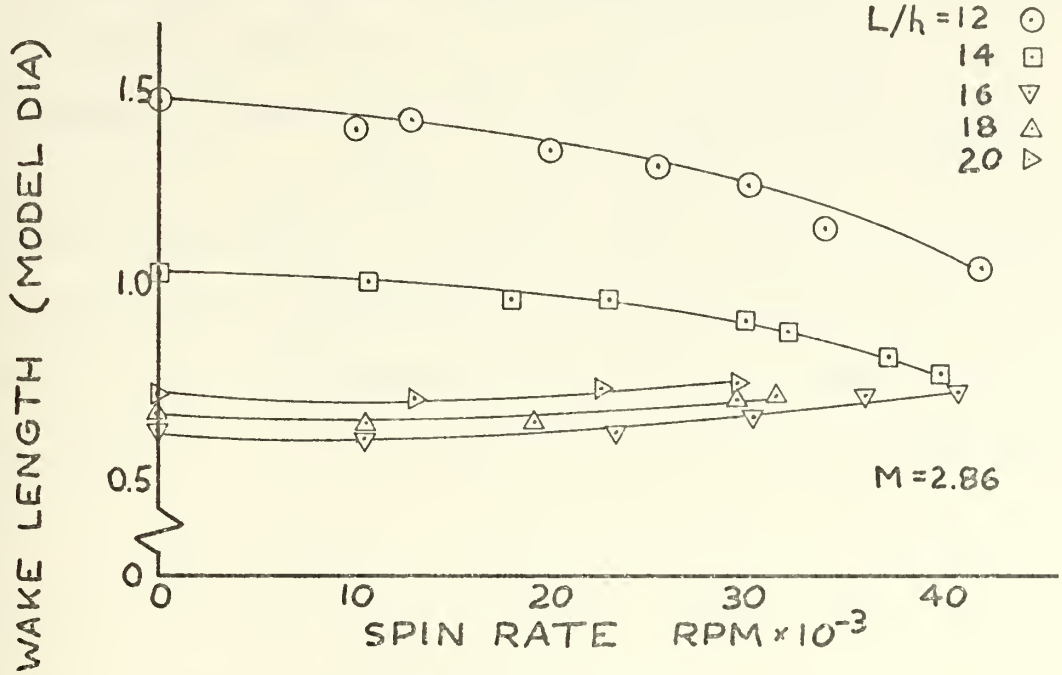

FIG. 9

WAKE LENGTH VS. MODEL SPIN RATE

REF. 9

E. HEAT ADDITION

Base drag reduction by external combustion was studied by W. C. Strahle [Ref. 13]. Strahle observed that the injection of mass or heat into the viscous recirculation bubble resulted in low efficiency since the base pressure rise was limited to the free stream atmospheric limit. Combustion in the inviscid supersonic stream, however, imposed no such limit and, therefore, showed the most promise for reducing the base drag or for providing a propulsive mechanism.

1. Control Volume Analysis

A control volume analysis [Ref. 6] as shown in Fig. 10 gives some intuitive feeling for heat addition in

the supersonic stream. Applying the momentum theorem for the control volume in the x direction, one has

$$(P_B - P_\infty)A_B = \int_d^e \rho u^2 dA - \int_b^c \rho u^2 dA + \int_c^d (P - P_\infty) dA + \int_d^e (P - P_\infty) dA \quad (1)$$

where dA is the projected area perpendicular to the free stream direction x. For planar flow and no heat addition, pressure P along streamline cd is determined by the local flow angle in accordance with the Prandtl Meyer function.

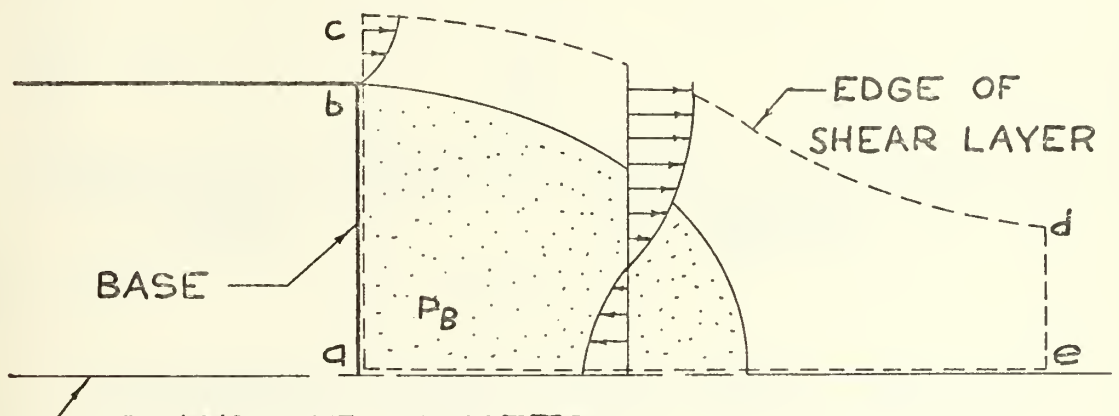

FIG. 10

BASE CONTROL VOLUME

Figure 11 shows that the static pressure has a lower value in the fast turning case (short recirculation region) as compared to the slower turning case (long recirculation region).

The $\int_c^d (P - P_\infty) dA$ will be less for a fast turning streamline; and, consequently, P_B also will be lower. Since by the continuity equation $\int_c^d \rho u dA = \int_d^e \rho u dA$, only changes in momentum

thickness δ^{**} and displacement thickness δ^{*} can change the momentum flux through de and bc, it is the gage pressure integrated over cd and de that largely determines base pressure.

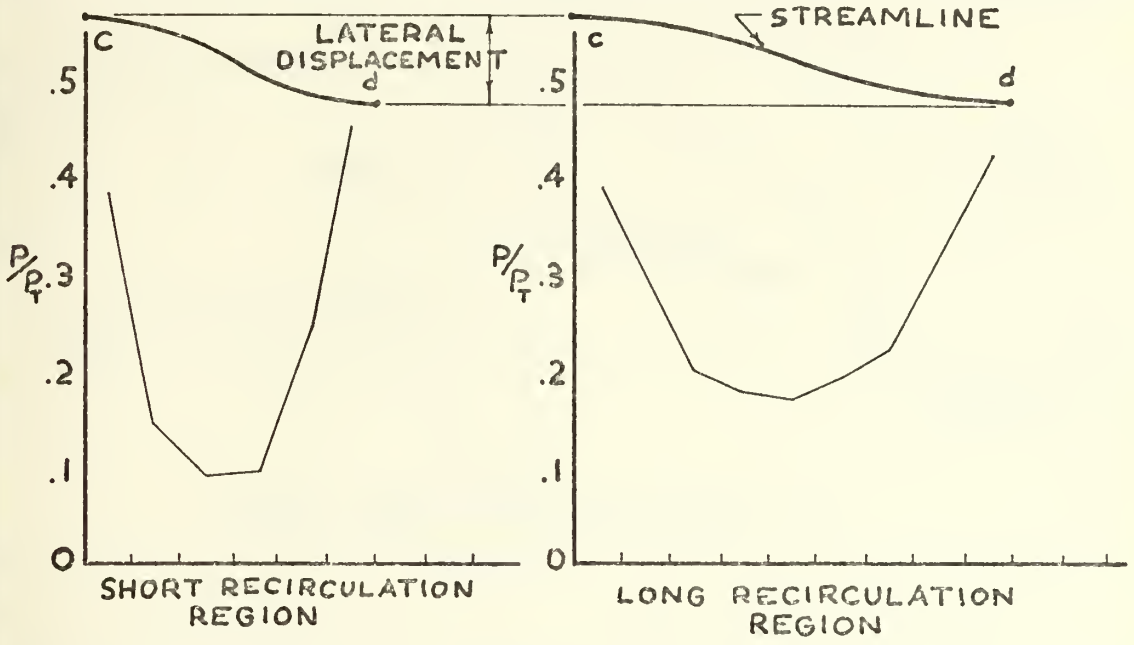

FIG. 11

PRESSURE ON SHEAR LAYER EDGE (REF. 6)

Compression waves emitted from the heat addition zone as shown in Fig. 12 increase the static pressure along the edge of the shear layer, cd in Fig. 11; and therefore, $\int_c^d (P-P_\infty)dA$ is increased thereby increasing P_B. The pressure decreases along cd as the flow turns toward the axis. By adding heat in the inviscid region, the shear layer is turned inward with no or less loss of static pressure along cd. P_B is increased which results in a base drag reduction.

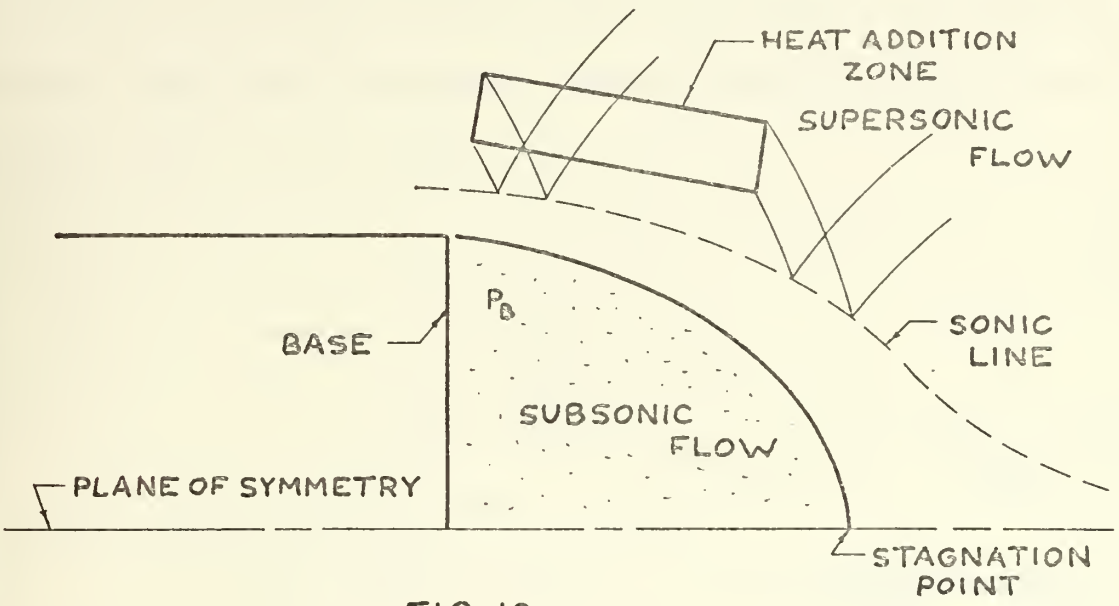

FIG. 12

HEAT ADDITION ADJACENT TO BASE

2. Strahle Two-Dimensional Model

Strahle [Ref. 13] restricted his heat addition model to two-dimensional, turbulent, supersonic flow, with the heat addition zone aligned with the inviscid stream beyond the base corner turn as shown in Fig. 13.

The heat addition zone is rectangular in shape and is assumed far enough removed from the viscous region to preclude any heated streamlines being entrained in the viscous flow region, which would result in a performance loss. Strahle chose the mixing theory of Crocco and Lees [Ref. 2] to describe the base flow because of the method's success in

predicting the base pressure. Strahle found that the inclusion of external combustion did not alter the base flow theory of Crocco and Lees but instead only changed the initial conditions for Crocco - Lees governing differential equation (Eq. 2.30 in [Ref. 2]).

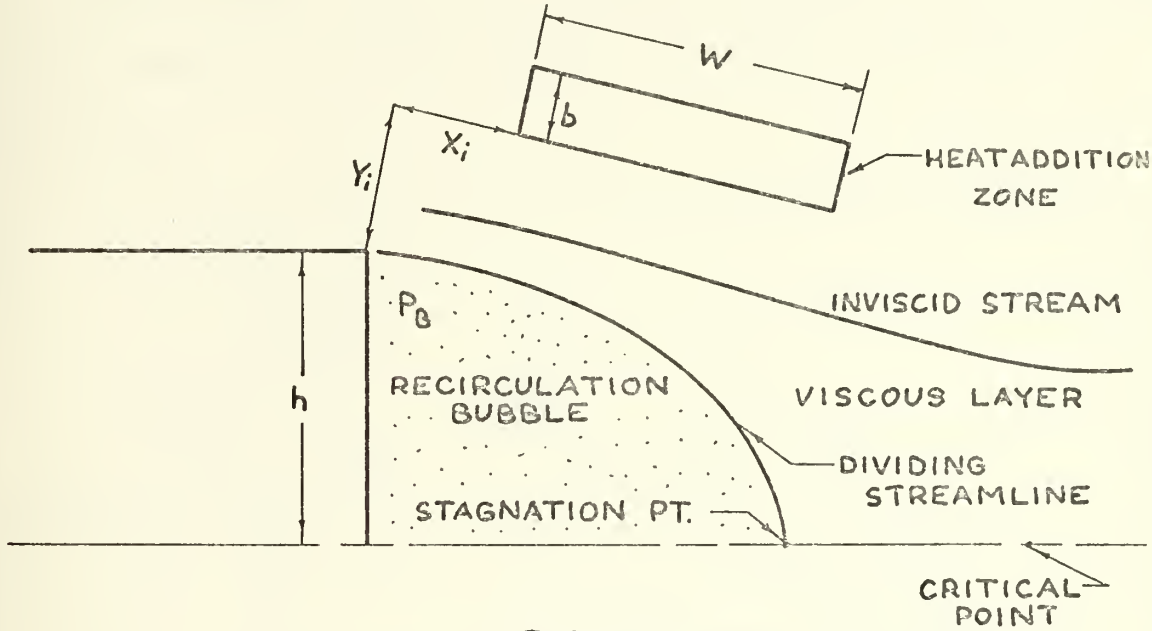

FIG. 13
STRAHLE MODEL FOR HEAT ADDITION

With heat addition, the angle of inclination Θ in Fig. 14 is no longer a function of W_e alone but is also a function of both W_e and x.

The symbol W_e is the ratio of the x component of velocity to the speed of sound a_t. A saddle point singularity exists through which the trajectory must pass in order that the far wake limit can be reached. This forms the uniqueness

condition; since without it, an infinite number of solutions would exist. This saddle point is called a critical point and physically represents the transition point from subsonic to supersonic flow in the viscous region. A unique solution is forced by the critical point regardless of the external combustion occurring in the inviscid stream. The position of the critical point, however, and the influence on the allowable initial condition will be altered since θ is influenced by combustion.

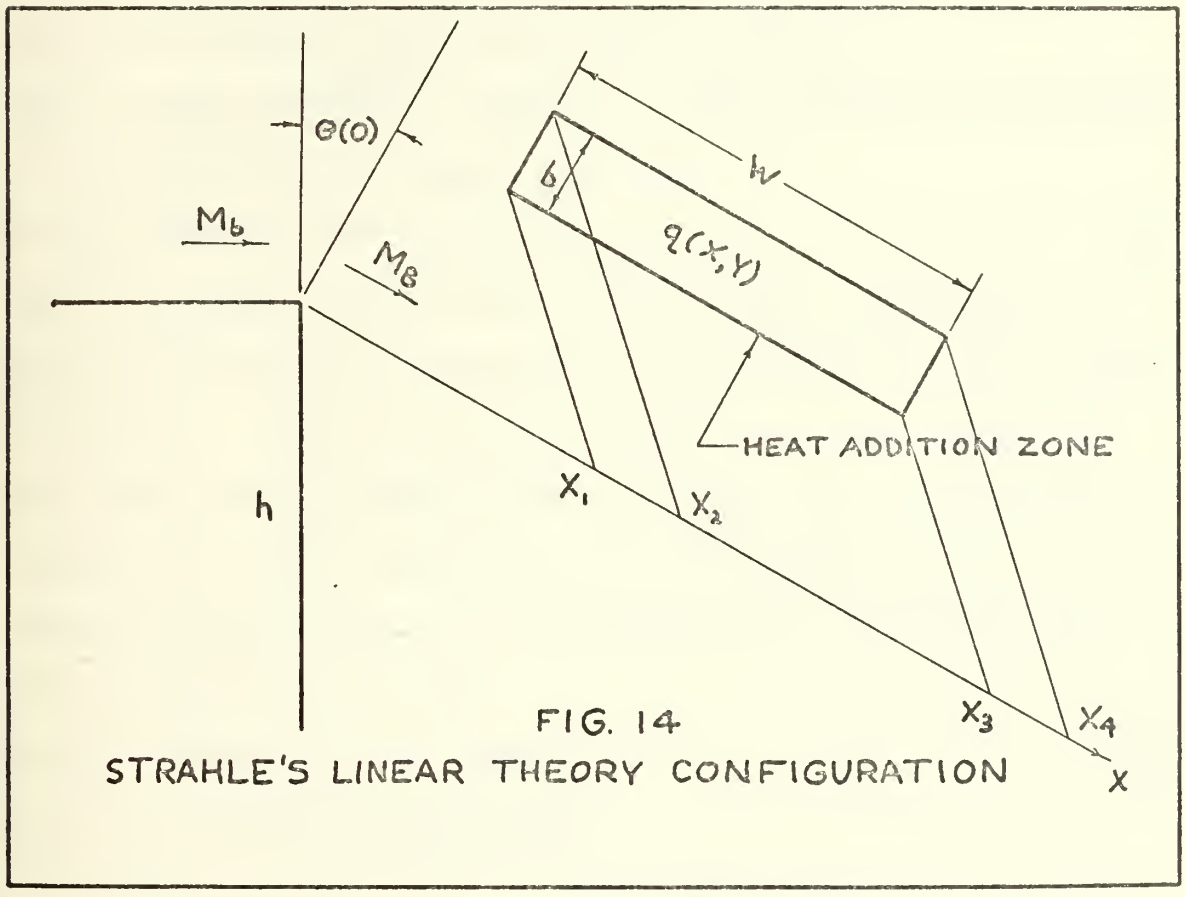

FIG. 14
STRAHLE'S LINEAR THEORY CONFIGURATION

Strahle analyzed the combustion region by the linear theory of heat addition applied to a supersonic stream. The X and Y coordinates defined in Fig. 14 are obtained by rotating the

axis through an angle $\Theta(o)$ and are aligned with the rectangular heat source. In the uniform field with Mach number equal to M_B, the perturbation velocity potential equation is

$$-\beta_B^2 \phi_{xx} + \phi_{YY} = f \equiv (\gamma-1) q / \rho_B a_B^2 \qquad (2)$$

and the pressure coefficient is $C_p = -2\phi_x/u_B$. Upon integrating Eq. (2) where f is non zero only for positive X and Y, along the Y = 0 line, the perturbation velocity potential is

$$\phi_x(X,o) = -1/\beta_B^2 \int_o^x f[x', (x-x')/\beta_B]\, dx'. \qquad (3)$$

With $\Theta(o)$ unknown and thus the orientation of q, which is the heat release per unit volume per unit time, also unknown, the Bernoulli equation along a streamline states

$$dP/\rho u^2 = -du/u = d\theta/\sqrt{M^2+1} - d\phi_x/u = -d(M^2)/2M^2[1+(\gamma-1)M^2/2] \qquad (4)$$

Solving for $d\Theta$ and integrating yields

$$\Theta - \Theta_b = \nu(M_b) - \nu(M) + \beta_B \phi_x/u_B \qquad (5)$$

where ν is the Prandtl Meyer function. ϕ_x is evaluated at $\Theta(o)$ on the Y=0 line regardless of the history of the viscous region edge. For large heat addition, this is a source of error since the initial direction of the viscous region is different from its alignment at the conclusion of the influence of heat addition. Integrating Eq. (3) and substituting into Eq. (5) gives

$$\Theta - \Theta_b = \nu(M_b) - \nu(M) - \eta g(x) \qquad (6)$$

where $\eta = (\gamma-1)\Delta h_f/\beta_B a_B^2 \pi W$

$$\begin{aligned} g(x) &= 0 && \text{if } x<x_1,\ x>x_4 \\ &= x - x_i - \beta_B Y_i && \text{if } x_1 \le x < x_2 \\ &= \beta_B b && \text{if } x_2 \le x < x_3 \\ &= \beta_B [Y_i + b - x + x_i + W] && \text{if } x_3 \le x \le x_4 \end{aligned}$$

with $X_1 = X_i + \beta_B Y_i$

$X_2 = X_i + \beta_B (Y_i + b)$

$X_3 = X_i + W + \beta_B Y_i$

$X_4 = X_i + W + \beta_B (Y_i + b)$

3. Strahle One-Dimensional Model

Because the linear theory contains contradictions of the assumptions at even modest levels of heat addition, Strahle suggested a one-dimensional approach for comparison. Figure 15 shows the basic scheme under a small angle assumption that $dA_h/dx \cong \theta_2 - \theta_1$ and $dA_e/dx \cong \theta_1 - \theta$ where A_h is the area of the heat addition zone and A_e is the area of the adiabatic free stream.

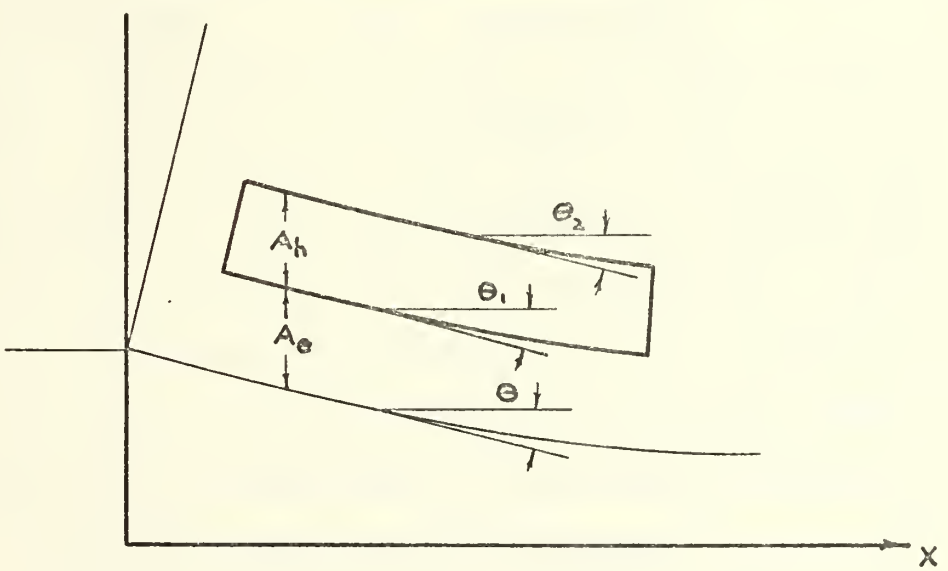

FIG. 15
STRAHLE'S ONE-DIMENSIONAL HEAT ADDITION

Assuming the flow on the upper side of A_h (Fig. 15) contains waves of only one family, then $\Theta_2 = \Theta_b + \nu(M_b) - \nu(M)$. Using the one-dimensional flow relations that $(dA_e/A_e)dx = (1-M_e^2)\gamma M_e^2 (dP_e/P_e)dx$, Strahle obtains

$$\Theta - \Theta_b = \nu(M_b) - \nu(M) - (A_e/P_e)\left[(1-M_e^2)/\gamma M_e^2\right] dP_e/dx - dA_h/dx. \quad (7)$$

dPe/dx is always maintained small by the combustion-affected region. Thus, for large heat release, dA_h/dx dominates the pressure gradient term. If $\eta\, g(x)$ is identified with dA_h/dx in Eq. (6), then an analogy exists between the one-dimensional and linear theory approaches. On the average, $dA_h/dx = b(\Delta V/V)/W$ where $\Delta V/V$ is the constant pressure volume expansion of the combustible mixture, b is the heat addition zone capture height, and W is the length of the combustion zone. With $g(x)$ assumed in the strongest region where $X_1 \leq X \leq X_2$ in Eq. (6), the equivalence is made that

$$\Delta V/V = (\gamma-1)\Delta h_f/\mathcal{M} a_\infty^2 \quad \text{and} \quad \eta = \Delta V/VW\beta_B \quad (8)$$

where Δh_f is the heat release per unit mass of fuel, $\mathcal{M}$ is the air to fuel ratio, and $\beta_b = \sqrt{M_b^2 - 1}$. Functionally, $\Delta V/V = f(\mathcal{M}, P_B, T_B)$ with the most important dependences being on $\mathcal{M}$ and T_B, which is the base temperature. Strahle hoped that by combining linear theory with a one-dimensional approach the features of both methods could be included while removing most of the objections of each method individually.

4. Strahle's Performance Parameters

Strahle computed the force on the base to be $F_B = 2(P_B - P_{B_o})h$ where P_B is the pressure on the base (where X = 0) and h is the base half height. The specific impulse is defined as $I_{sp} = F_B/\dot{m}_f$ where $\dot{m}_f$ is the fuel flow rate.

For small values of force level on the base and letting $M \to \infty$

$$I_{sp} = [2\Delta h_f(\gamma-1)/\gamma M_B \beta_B bW](P_B/P_b)(dP/d\eta) \qquad (9)$$

where $P = P_B/P_b$ and η = a heating parameter. The fact that $M \to \infty$ creates an absolute linear heat addition limit, which though impractical, does suggest the strong role that the critical point plays in the nonlinear regime.

Figure 16 shows the effect the heat addition zone location has on specific impulse. As X_i is moved from the base toward

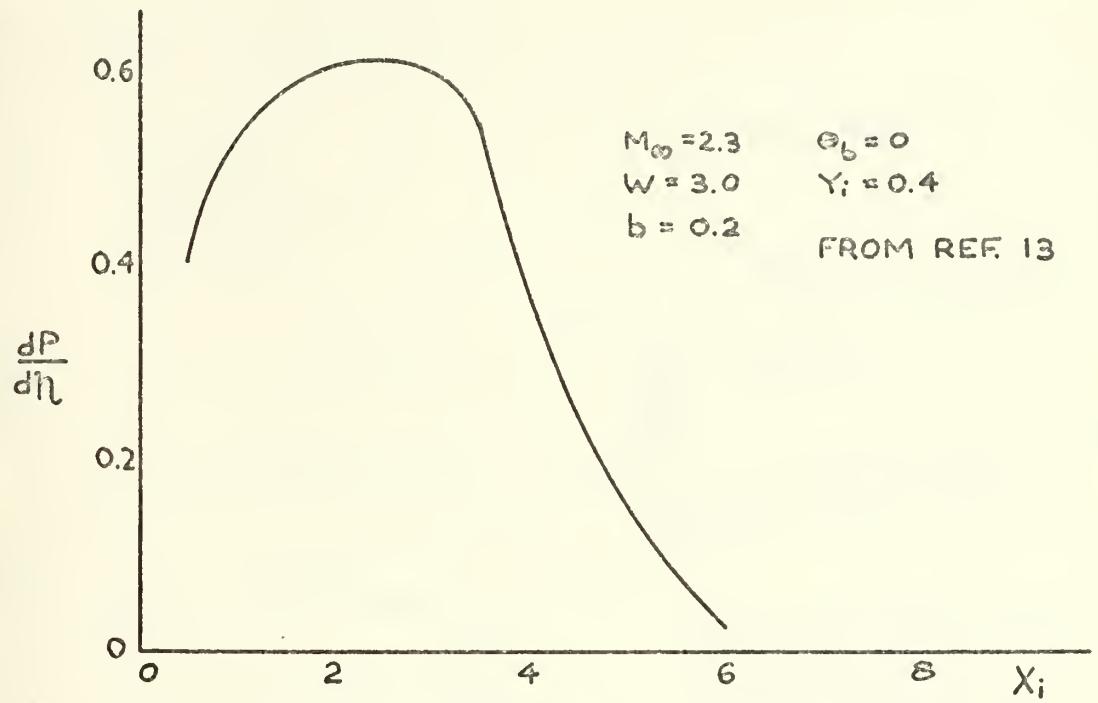

FIG. 16

STRAHLE'S SMALL DISTURBANCE SPECIFIC IMPULSE $dP/d\eta$ VS. COMBUSTION ZONE LOCATION X_i

the critical point, which is located at approximately x = 7.7 in the linear limit, the specific impulse $(dP/d\eta)$ reaches a maximum when the combustion zone is roughly centered between the base and the critical point. A steep drop in effectiveness occurs as the zone nears the critical point and extends

beyond it. This is expected because any influence upon the reattachment process downstream of the critical point where the flow is supersonic cannot be transmitted upstream. The linear limit predicts that external combustion will result in a base pressure rise, the specific impulse is expected to be high, and the combustion is wasted if the length of the heat addition zone W is too long.

Strahle recomputed the example in Fig. 16 for finite combustion strength, and the resulting axial pressure distributions are shown in Fig. 17.

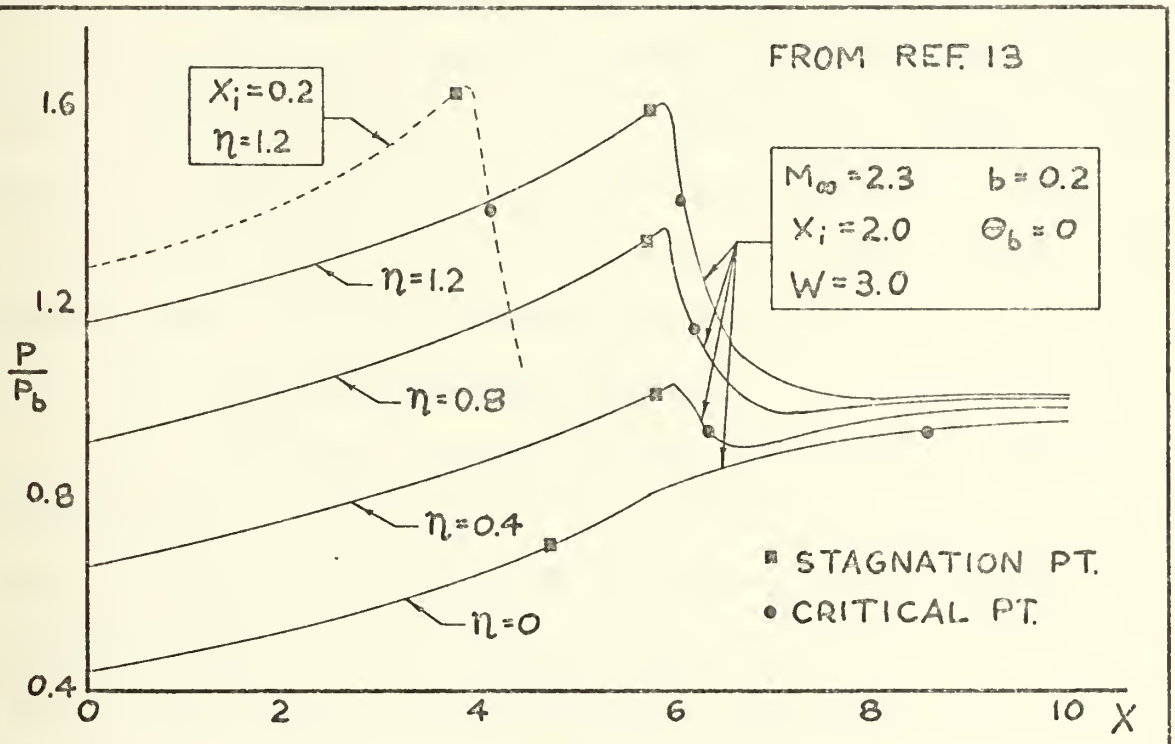

FIG. 17
STRAHLE'S FINITE AXIAL PRESSURE DISTRIBUTIONS

Four of the curves are for $X_i = 2.0$ which corresponds to the maximum I_{sp} location in Fig. 16. The top curve is for $X_i = 0.2$. Apparently, for this case, it is best to have X_i small. The reason for this lies in the nonlinear behavior

of the critical point. In all cases, the critical point becomes entrained in the expansion portion of the combustion-affected zone. The combustion length W, therefore, fixes the interaction length, and Strahle suspected that the most efficient placement of the combustion region would be as close to the base as possible. He also reasoned that the base pressure increase resulted from the entrapment of the subsonic recirculation bubble by compression waves emitted by the combustion zone. The singularity can occur only when the inviscid flow is directed inward or for $\Theta < 0$. The viscous zone thickness, however, must remain finite. Since the primary effect of the combustion region is the downward turning of the flow, the last available position for the critical point appears to be within the combustion-affected portion of the flow. The flow passing the base corner cannot turn as far without combustion, which in turn indicates a rise in base pressure.

5. Axisymmetric Heat Addition

Strahle's two-dimensional heat addition requires modification for axisymmetric application. A method by Fuhs [Ref. 6] suggests that the change in base drag resulting from external burning is $\Delta D_B = \Delta P_B A_B$ where A_B is the area of the base for both planar and axisymmetric bodies as shown in Fig. 18.

Equal amounts of heat are released in both the planar and axisymmetric cases. Heat addition in the planar case is represented by the lines above and below the base area and in the axisymmetric case by a concentric circle of radius r_2. Since in both cases, the length of heat addition zone is

$2\pi r_2$, the base area influenced by heat release is in the ratio

$$\frac{\text{axisymmetric base area}}{\text{planar base area}} = \pi r_1^2 / 2\pi r_1 r_2 = r_1 / 2 r_2 \qquad (10)$$

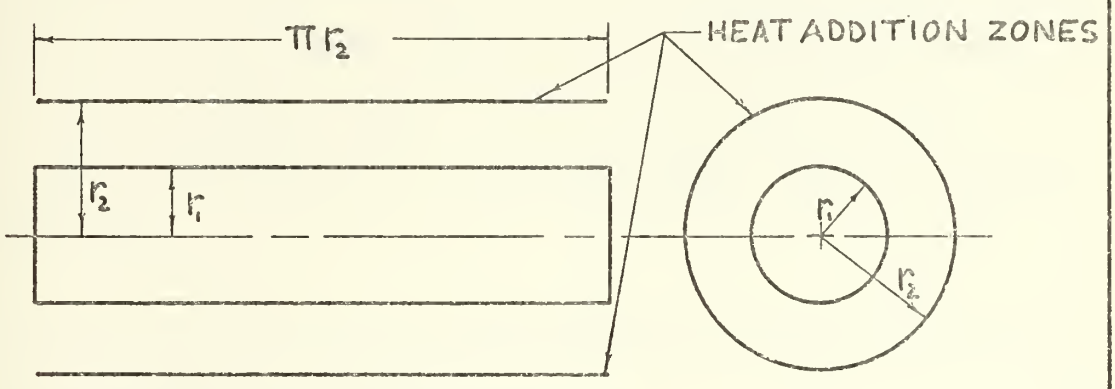

FIG. 18
COMPARISON OF BASE AREA FOR PLANAR AND AXISYMMETRIC GEOMETRY

The axisymmetric geometry apparently has less base area influenced by heat addition. Flow through an annular heat addition region was investigated. It was found that the compression waves merged sooner with axial symmetry, and that in contrast with the planar case, there is an optimal r_2/r_1 ratio.

III. APPARATUS

In order to study the effects of heat addition on the base pressure of an axisymmetric body, a free jet wind tunnel was constructed at the Naval Postgraduate School's blow down laboratory. The test model simulated a 5-inch projectile at 23,000 feet and a Mach number of 2.0, which are typical conditions for a maximum range trajectory. Similarity parameters were matched by using a Mach 2.0 free jet coaxial nozzle shown in Fig. 19 which gave a Reynolds number based on radius of 1.51×10^6.

FIG. 19
COAXIAL CYLINDER/NOZZLE

A turbulent boundary layer was assumed, and the displacement thickness δ^* was computed to be 0.041 inches at the projectile base. This provides a similarity parameter of displacement thickness to radius δ^*/h of 0.0164.

The equipment consists basically of a 300 psig air supply, a globe valve, a pressure reducer valve, a 90° elbow, a center cylinder support/flow straightening section, a nozzle and an overhead exhaust hood. A 4-inch pipe feeds the air from the supply tank to the on/off globe valve. The pressure reducer valve is followed by a 90° elbow which directs the air flow vertically and provides a feedback pressure for the regulation of the pressure reducer valve. A 2-inch spacer is located between the elbow and the center cylinder support section and provides internal access to the centerline cylinder. The centerline cylinder is supported inside the center cylinder support section by flow straighteners located at the top and bottom of the 3-foot section of 4-inch pipe. A section of 6-inch pipe houses the nozzle on top of the cylinder support section and provides armor protection and a support for the pressure probe as shown in Fig. 20. Figure 21 shows the exhaust hood above the apparatus, the mercury manometer board used to obtain pressure data, the mercury vapor light source and one mirror used in the schlieren system for flow visualization.

Figure 22 shows the cylinder extending from the cylinder support section with the nozzle and armor section removed, along with the pressure gage connected to the air supply reservoir.

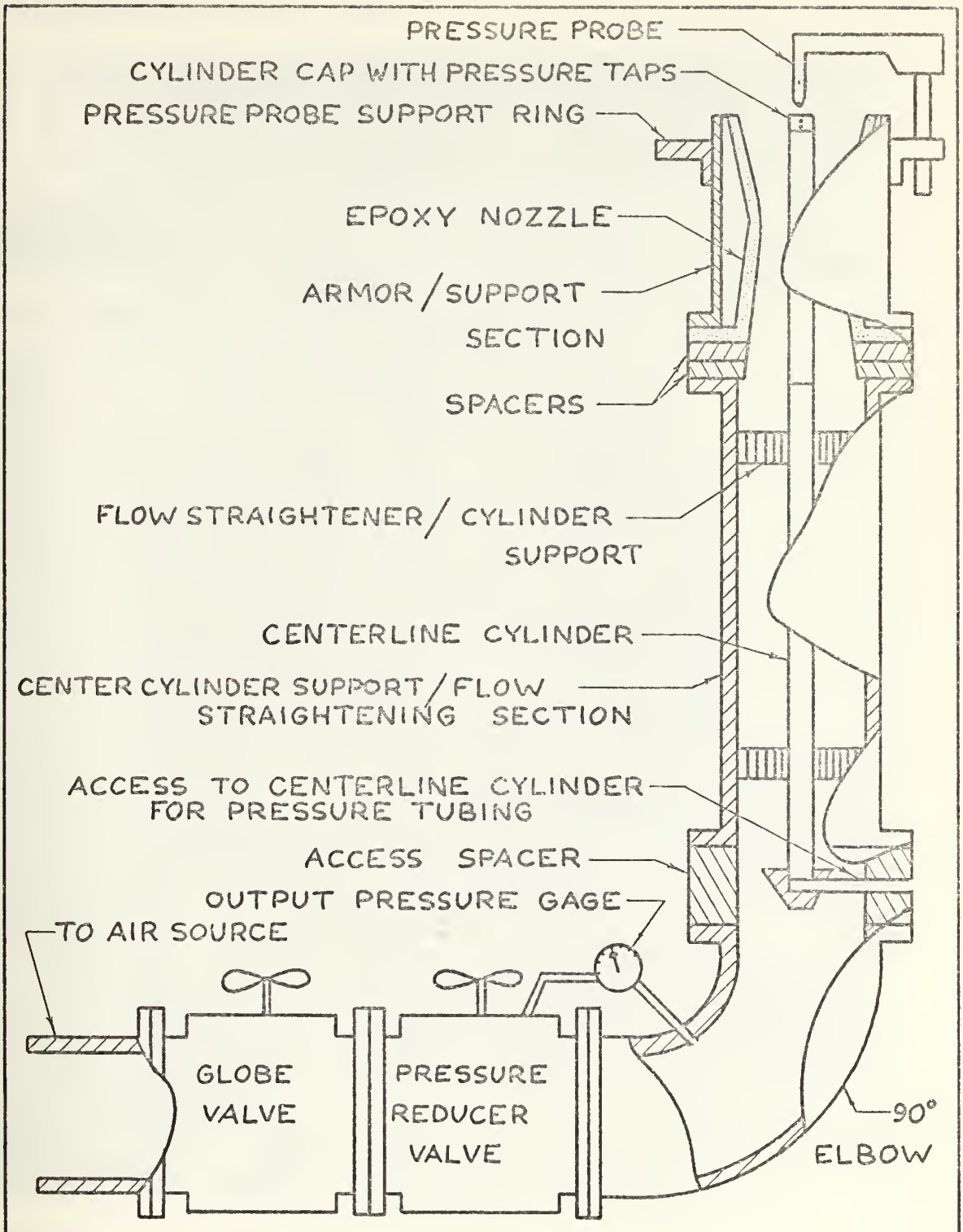

FIG. 20
TEST APPARATUS

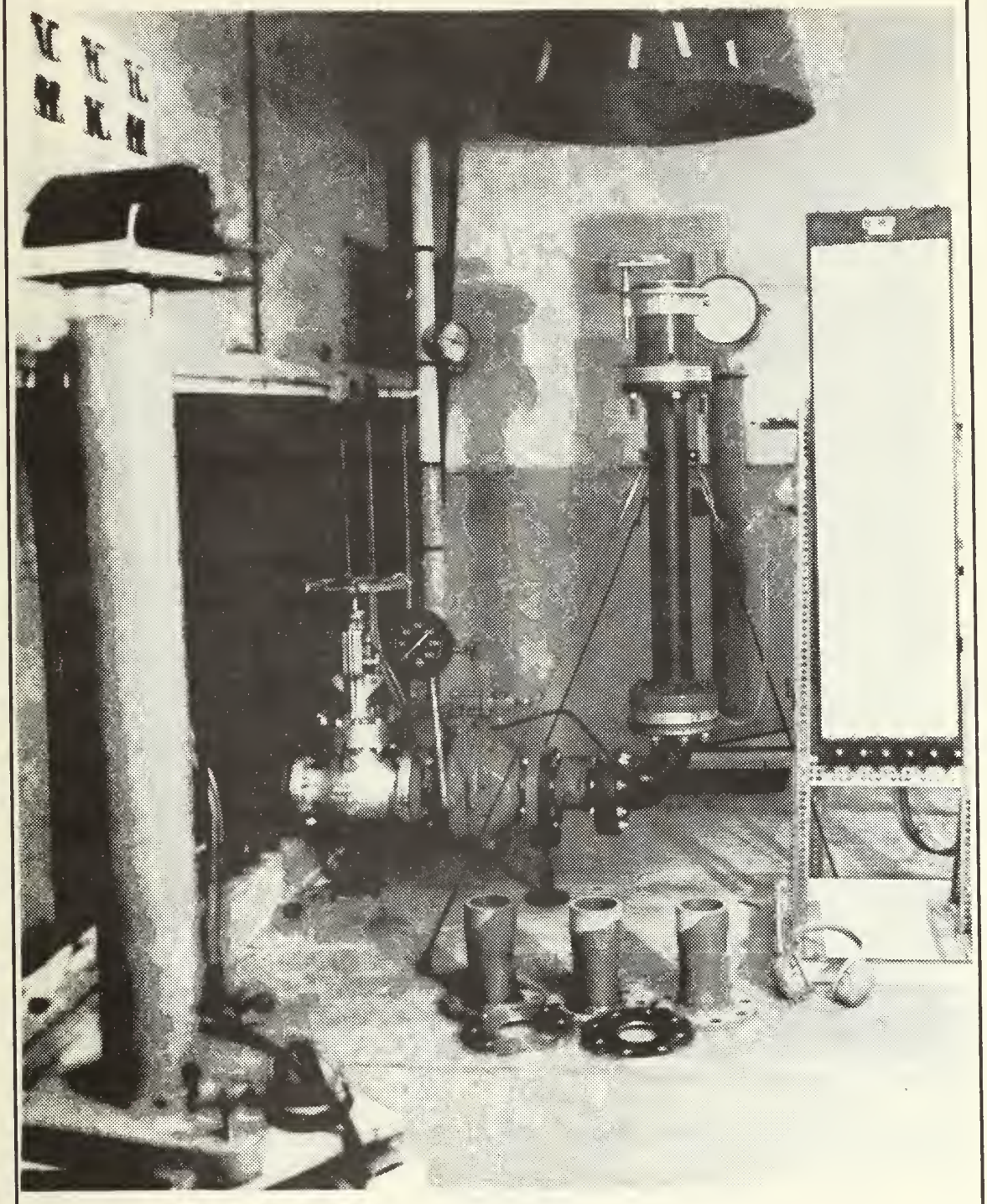

FIG. 21
PHOTOGRAPH OF TEST APPARATUS

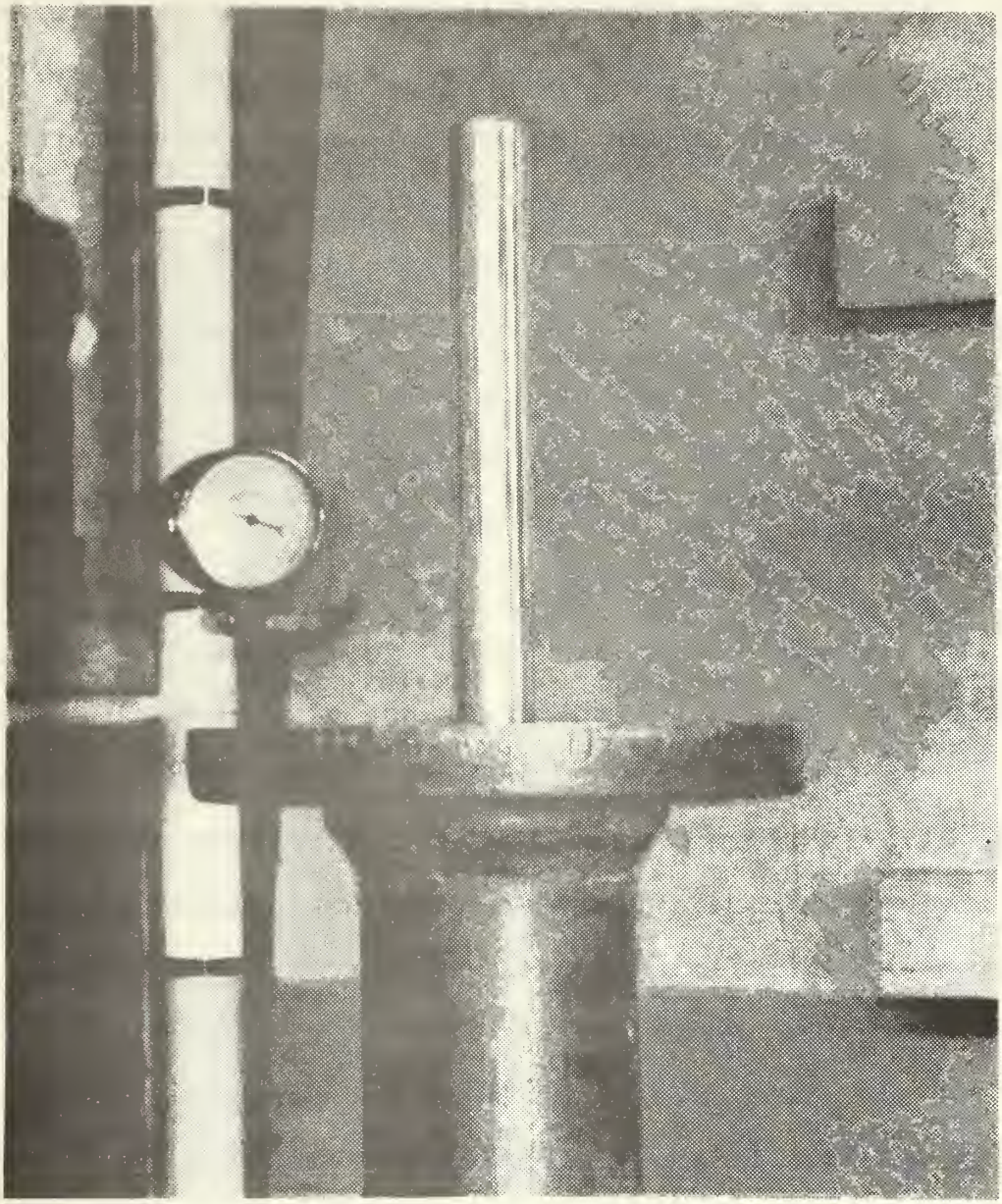

FIG. 22

TEST CYLINDER

The cylinder base is formed by a cap which contains six pressure taps. Four taps are located across the base radius, and two taps are located just upstream of the base corner.

The pressure from each tap is carried downward through the cylinder and the cylinder support in plastic tubes which exit the apparatus through the 2-inch spacer located on top of the elbow. The tubes are connected to a mercury manometer from which the pressure data was read. Total and static pressure also can be measured by the external pressure probe, which will be the primary base pressure source when cylinder spin is included. The results of this study were for the static case with all similarity parameters matched except for spin. However, because spin appears to have a considerable importance on base pressure, provisions were included to allow spinning the projectile. When a 5-inch projectile is fired, the barrel rifling spins the projectile to 250 revolutions per second. This establishes a spin similarity parameter of $r\omega/u = 0.1595$ where r is the radius of the projectile, ω is the angular velocity and u is the free stream velocity at Mach 2.0 at 23,000 feet altitude. The similarity parameter will be matched in the free jet experiment by spinning the cylinder at 48,000 rpm. The spinning cylinder design consists of a 6.5-inch stainless steel cylinder which slides over a support cylinder containing high pressure nitrogen orifices to provide gas bearing support and align the spinning cylinder radially. A small internal impulse turbine driven by high pressure nitrogen will spin the cylinder.

Heat addition was simulated by nozzle contour. As described in Ref. 6, the external burning process can be simulated by nozzle wall contours which generate characteristics identical to the supersonic combustion of an external burning assisted projectile. A gas generator within the projectile injects fuel-rich, hot, combustible mixtures into the supersonic inviscid flow where ignition occurs due to high temperature and the chemical nature of the fuel. The region of heat addition was assumed axisymmetric about the cylindrical body of the projectile with the radius r_2 in Fig. 18 equal to the body diameter. For stoichiometric fuel mixtures, calculations showed that the combustion would result in a 4.5° deflection of the streamline bounding the heat addition zone, and it was this 4.5° deflection inward of the streamline at r_2 from the cylinder centerline which governed the wall contour. Half stoichiometric nozzles also are planned for future analysis. An iterative procedure using the method of characteristics was used to design the nozzles to give the proper -4.5° flow angle. Using W to denote the length of the combustion zone (see Fig. 14) and h, the cylinder radius, several nozzles of varying W/h were fabricated with an epoxy cast poured over a wax plug to the correct contour. These nozzles provide several data points shown in Table I which show the effect external heating has on base pressure. During testing, spacers were used to vary the axial location of the heat addition zone with respect to the base corner. Figure 23 is a photograph of the nozzles, spacers, and tunnel armor section.

W/h / ℓ/h	0.72	1.84	4.34
-2.23	0.703	0.6	1.145
-0.95	0.685	0.858	1.258
-0.5	0.759	0.96	1.20
0.0	0.893	1.055	1.14
0.5	0.993	1.074	1.085

P_B/P_∞

TABLE I
TEST MATRIX

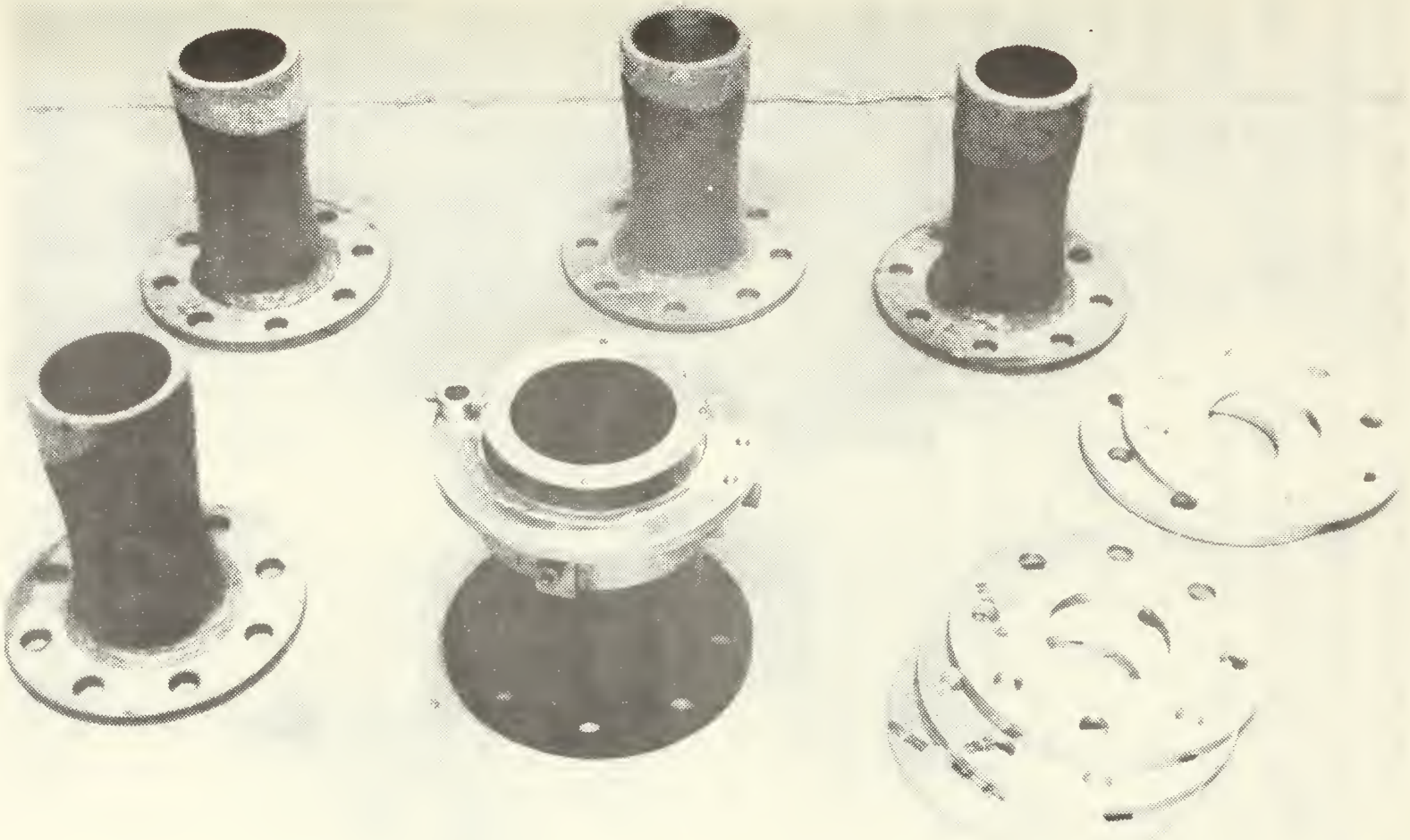

FIG. 23
PHOTOGRAPH OF NOZZLES, SPACERS, AND TUNNEL ARMOR SECTION

The symbol l represents the distance from the corner where the first fully developed compression wave impinges the cylinder wall or the wake downstream of the base, and h again is the cylinder radius as shown at the top of Figs. 40, 41, and 42. Five l/h values were observed for each nozzle as shown in Table I. Negative l/h denotes compression beginning upstream of the base corner, positive l/h signifies compression beginning downstream of the corner, and 0 denotes compression starting at the corner. Table I is the test matrix obtained to date showing the results of the completed tests.

IV. TEST PROCEDURE

After the proper nozzle and spacer combination was installed on the apparatus and the air reservoir was charged to 300 psig, a data point for the test matrix was taken. The procedure involved opening the globe valve and setting the proper output pressure from the pressure reducer valve. A pressure tap in the elbow was connected to a separate pressure gage which was used to set the conditions for each run. This tap also provided feedback pressure for the pressure reducer valve. With the proper output pressure set, a schlieren concave mirror system was used to photograph each test run as shown in Figs. 25-39. Polaroid positive/ negative film was used in order to facilitate print reproduction. Base pressure information was read from a mercury manometer and recorded for data reduction. At the conclusion of the data readings, the pressure reducer valve was turned off, and the air reservoir was recharged for the next run.

V. RESULTS AND CONCLUSIONS

The pressure ratios (P_B/P_∞) as shown in Table I indicate the performance of the observed simulated external burning. Figure 24 is a plot of the results.

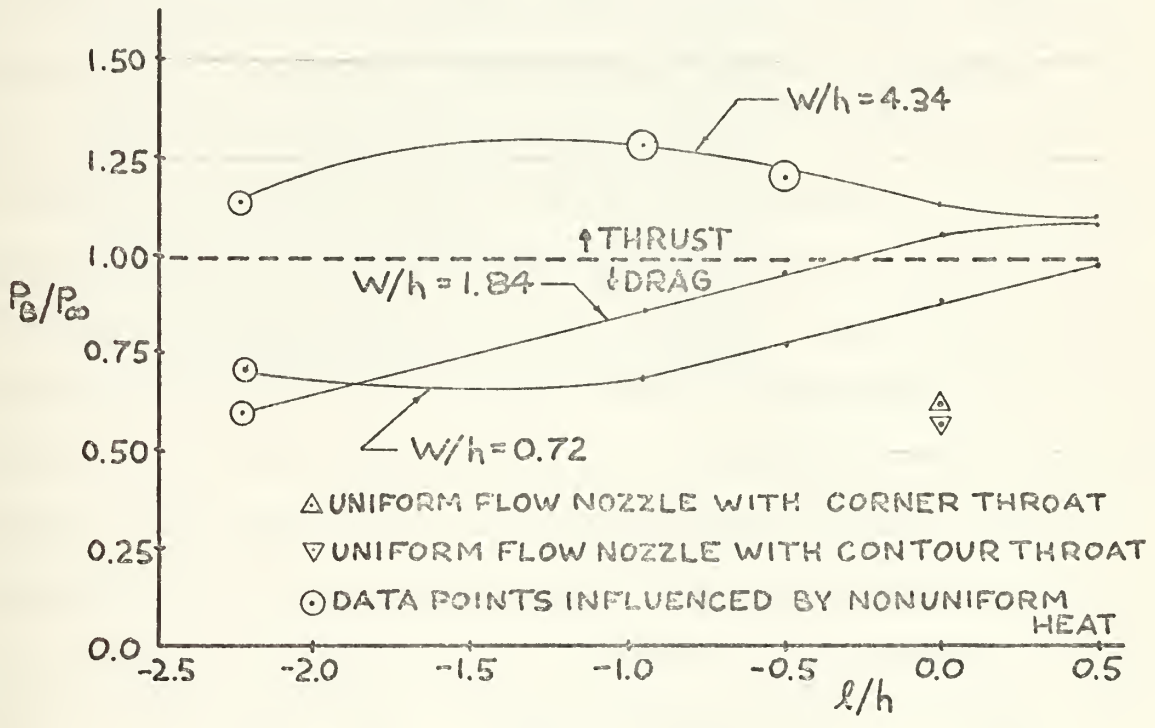

FIG. 24
P_B/P_∞ VS. ℓ/h FOR VARYING W/h NOZZLES

The data points taken for the two uniform flow nozzles compare favorably with M = 2 results compiled by Przirembel and Page [Ref. 10]. These points represent the base pressure ratio of the cylinder with no heat addition; and because P_B/P_∞ is less than 1.0, base drag results. All other data points, except one, show an increase in base pressure ratio with the applied combustion, indicating a reduction in base

drag. All the data for W/h = 4.34, and the last two points for W/h = 1.84 in fact, indicate thrust developed at the base since P_B/P_∞ for these cases is greater than 1.0. The data indicate, as expected, that a longer heat addition zone (Larger W) will result in a higher P_B/P_∞ increase, since a longer interaction length of compression waves acting upon the recirculation bubble has more effect than a shorter zone. It also appears that maximum benefit from the heat addition occurs when the entire recirculation bubble is embedded in the combustion-created compression waves. For W/h = 4.34, a decline in performance is noted as l/h exceeds -1.0, which indicates that for a long heat addition zone, optimal axial placement is necessary so as to not waste compression waves downstream of the sonic point. Because supersonic flow exists downstream of the sonic point, any compression effect occurring beyond that point will not be transmitted upstream into the subsonic circulation bubble, which would be necessary for a base pressure increase. For the shorter heat addition zones (W/h = 1.84 and 0.72), the base pressure ratio increases as the zone is moved rearward. It is assumed that no compression was wasted beyond the sonic point up to l/h = 0.5. Although not tested, a decline in performance is expected with further rearward movement of the heat addition region with respect to the cylinder base corner. Figures 25-39 show a schlieren-derived photograph of each data point obtained with a pictorial description of the heat distribution actually simulated. The double cross-hatched regions depict anomalous compression, and the single cross-hatched areas show the heat addition zones without multiple reflection.

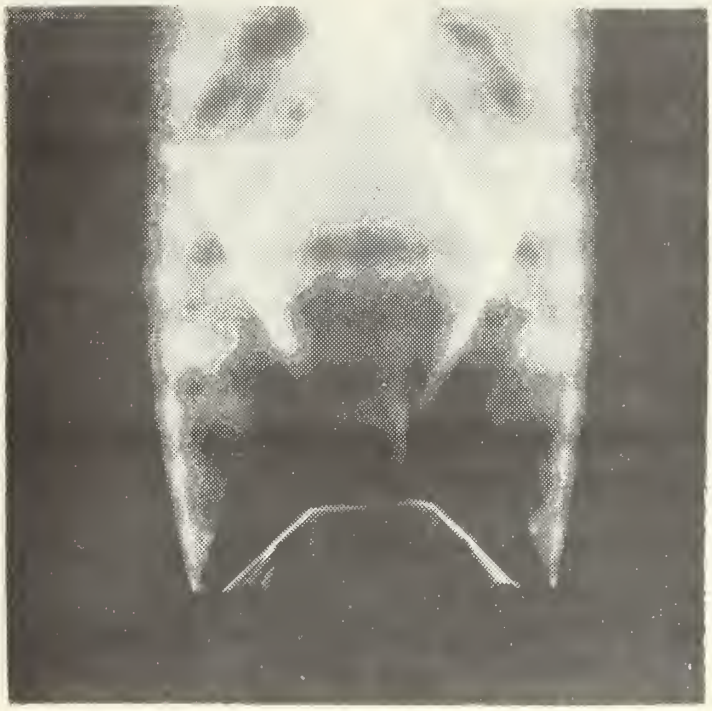

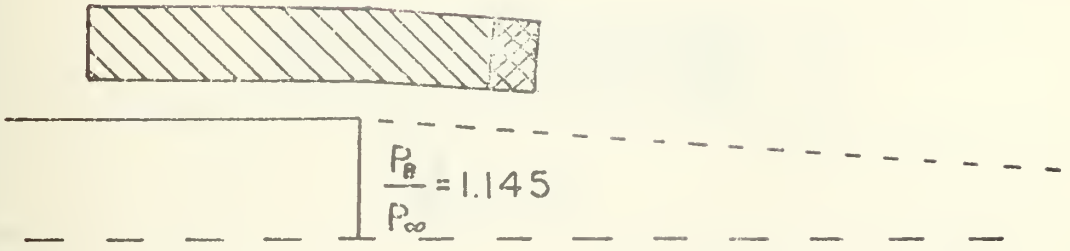

FIG. 25

PHOTOGRAPH AND SCHEMATIC FOR $W/h = 4.34$, $\ell/h = -2.23$

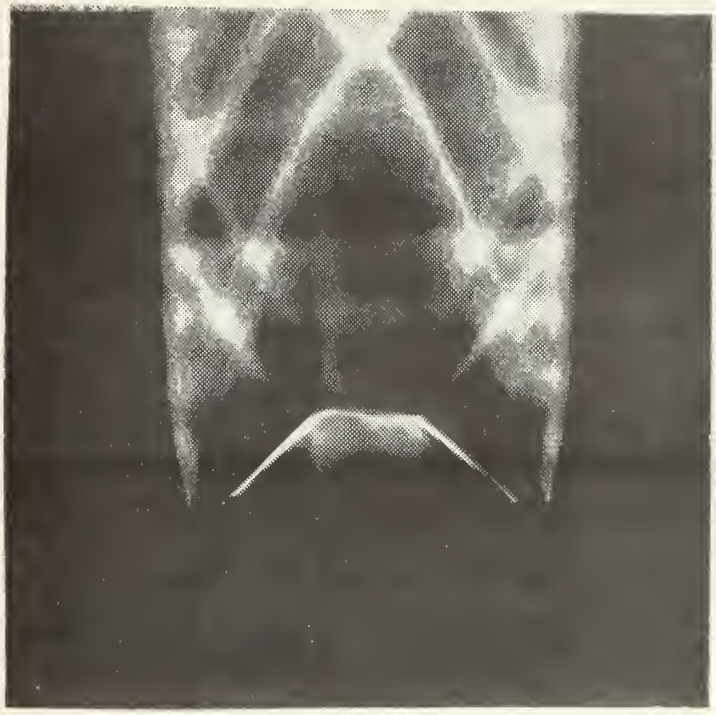

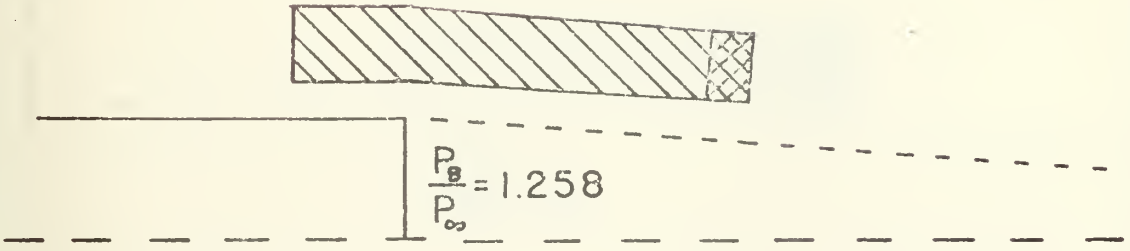

FIG. 26

PHOTOGRAPH AND SCHEMATIC FOR $W/h = 4.34$, $\ell/h = -0.95$

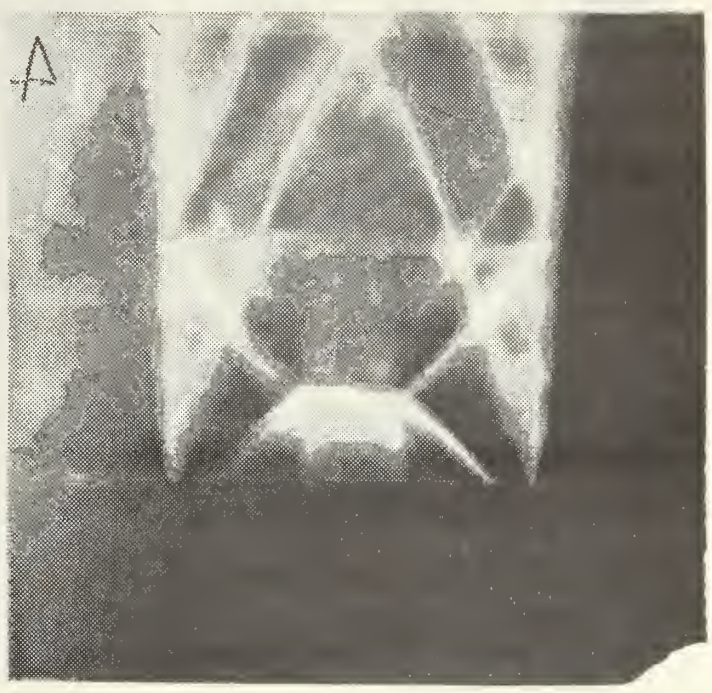

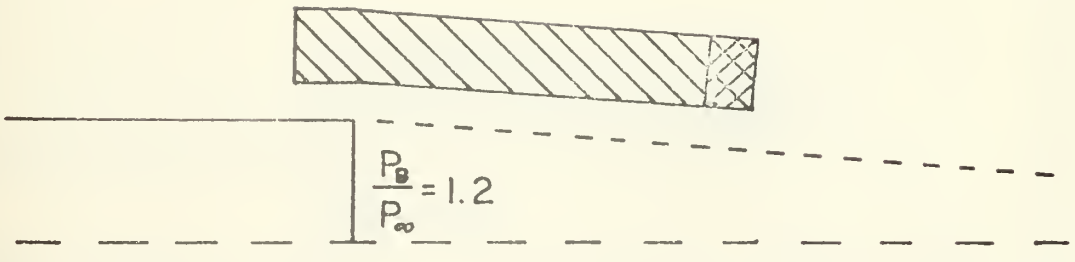

FIG. 27

PHOTOGRAPH AND SCHEMATIC FOR $W/h = 4.34$, $\ell/h = -0.50$

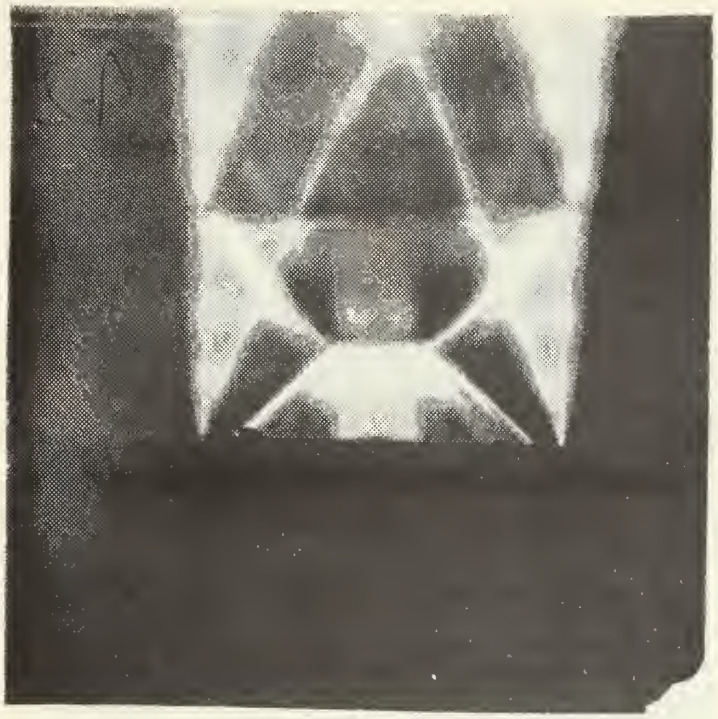

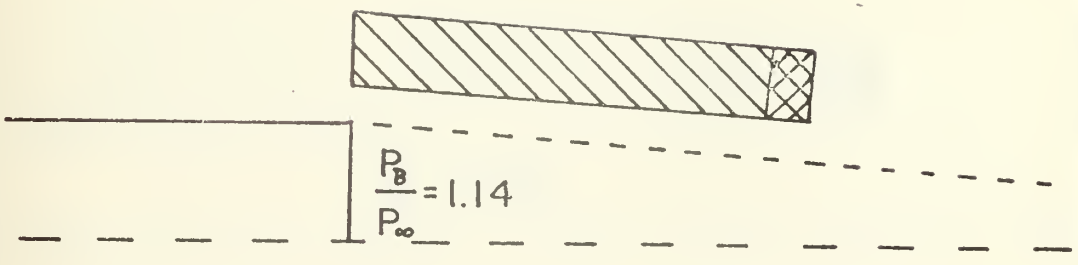

FIG. 28
PHOTOGRAPH AND SCHEMATIC FOR $w/h = 4.34$, $\ell/h = 0.0$

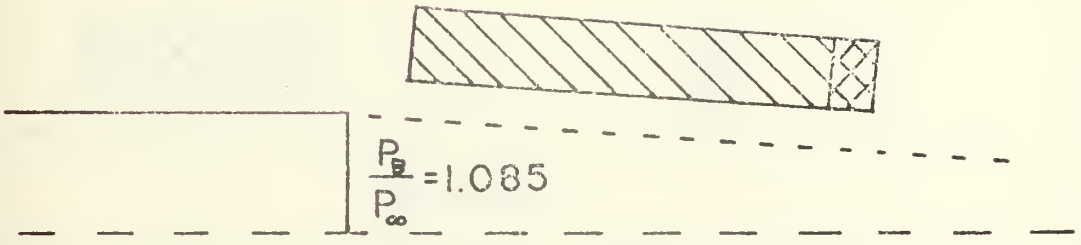

FIG. 29
PHOTOGRAPH AND SCHEMATIC FOR $W/h = 4.34$, $\ell/h = 0.50$

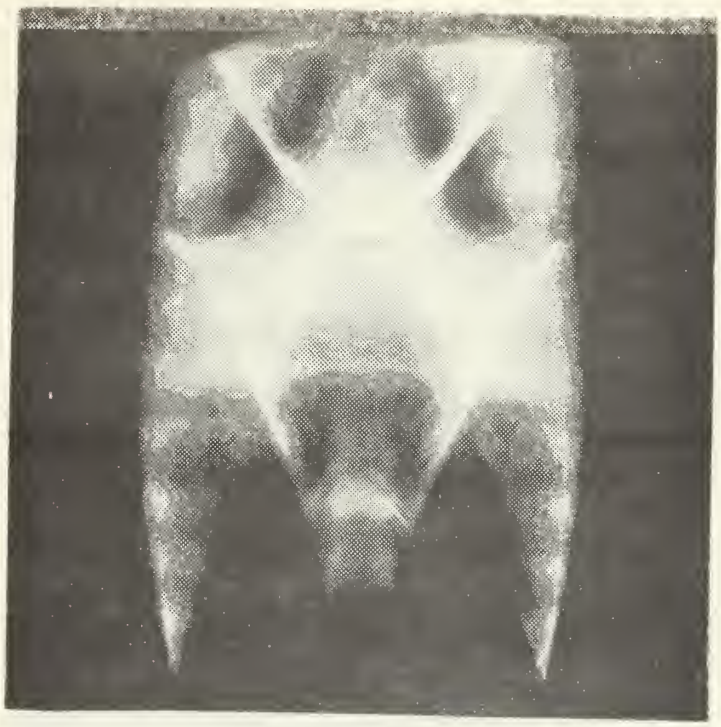

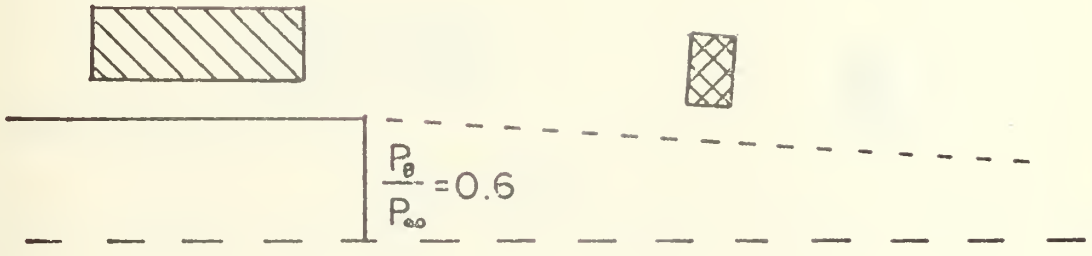

FIG. 30

PHOTOGRAPH AND SCHEMATIC OF $W/h = 1.84$, $\ell/h = -2.23$

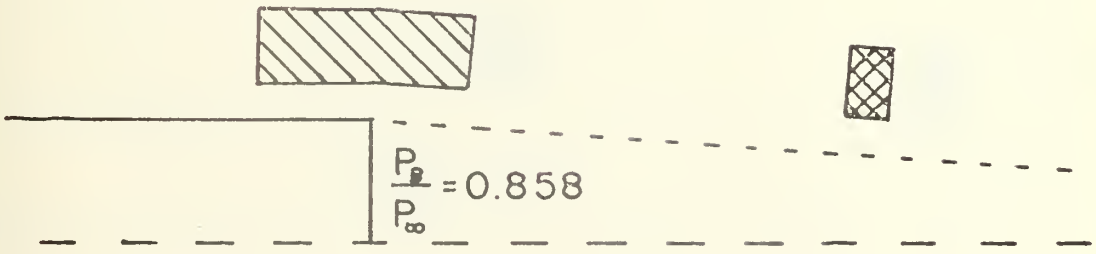

FIG. 31

PHOTOGRAPH AND SCHEMATIC FOR $W/h = 1.84$, $\ell/h = -0.95$

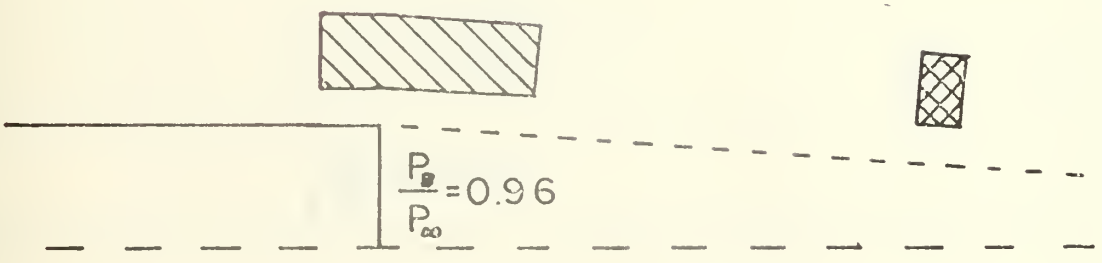

FIG. 32

PHOTOGRAPH AND SCHEMATIC FOR W/h=1.84, ℓ/h=-0.50

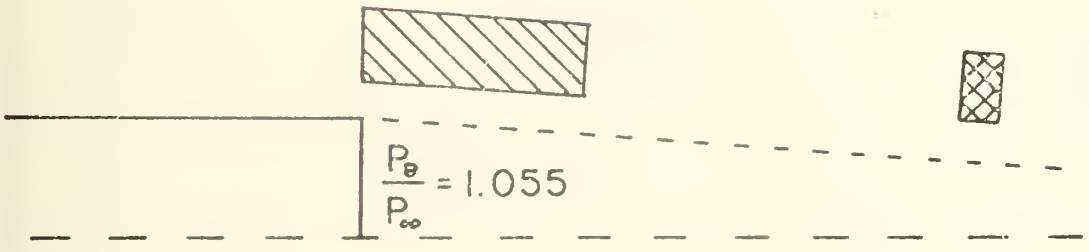

FIG. 33

PHOTOGRAPH AND SCHEMATIC FOR $W/h = 1.84$, $\ell/h = 0.0$

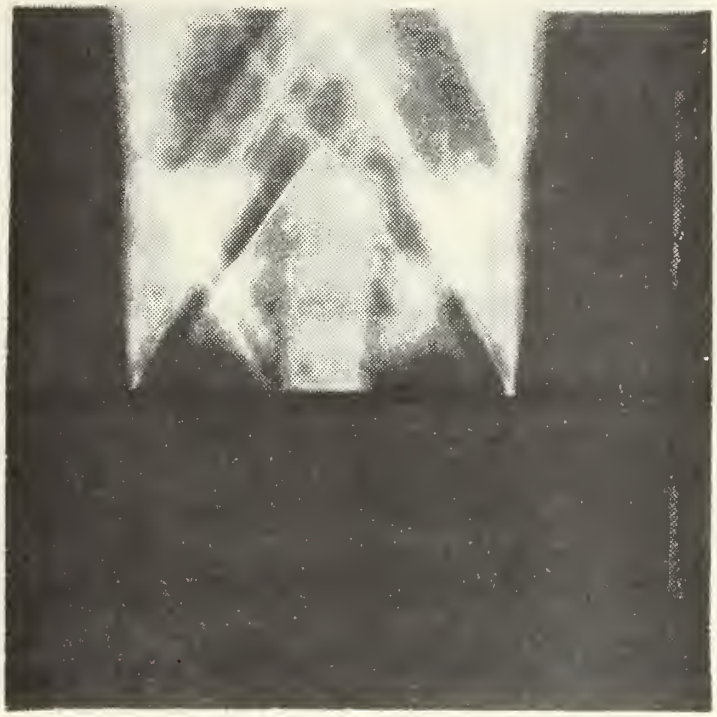

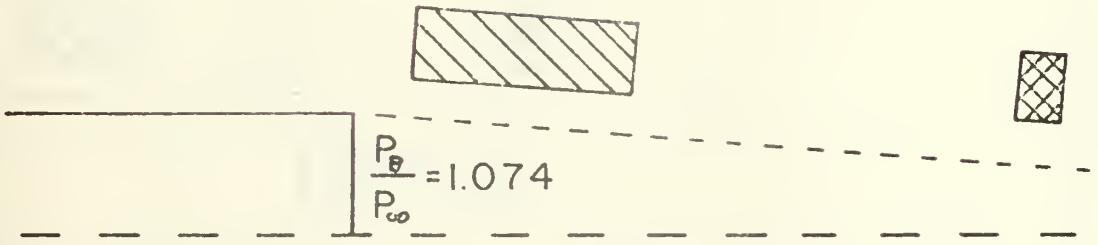

FIG. 34

PHOTOGRAPH AND SCHEMATIC FOR $W/h = 1.84$, $\ell/h = 0.50$

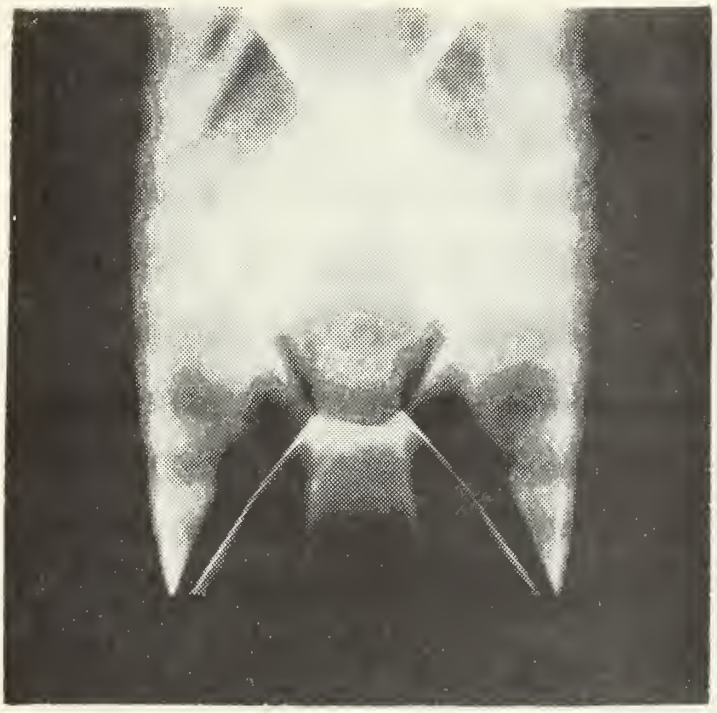

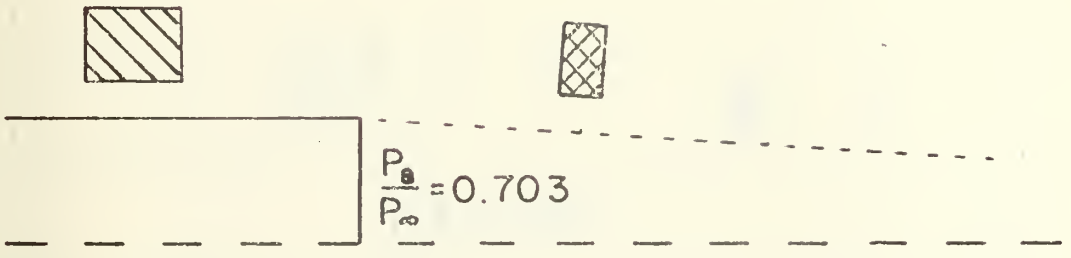

FIG. 35

PHOTOGRAPH AND SCHEMATIC FOR $W/h = 0.72$, $\ell/h = -2.23$

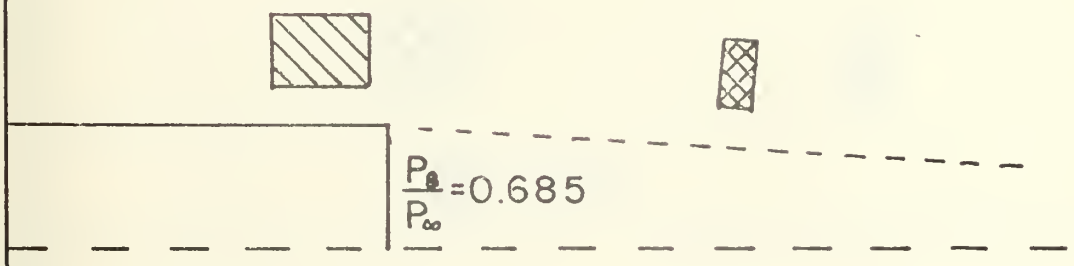

FIG. 36

PHOTOGRAPH AND SCHEMATIC FOR W/h=0.72, ℓ/h=-0.95

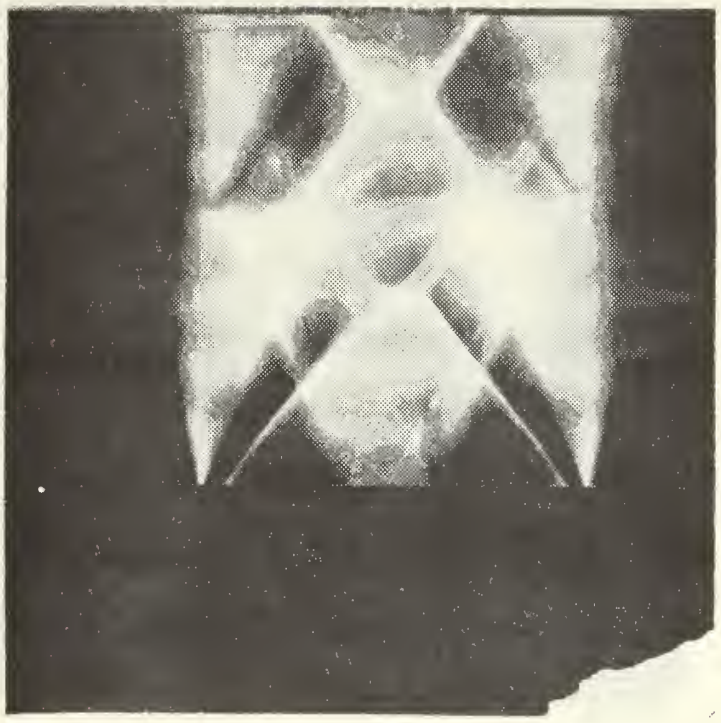

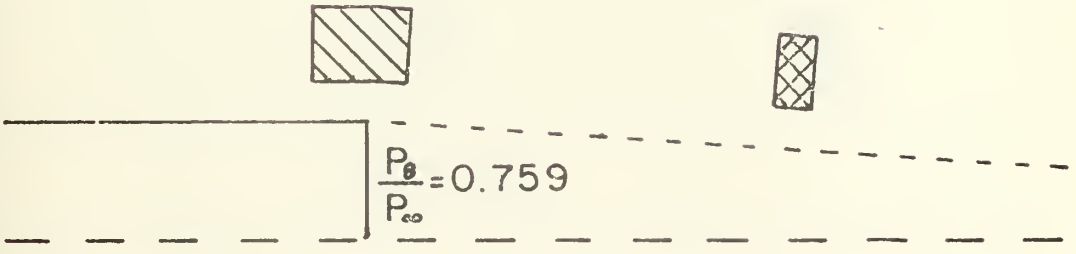

FIG. 37

PHOTOGRAPH AND SCHEMATIC FOR $W/h=0.72, \ell/h=-0.50$

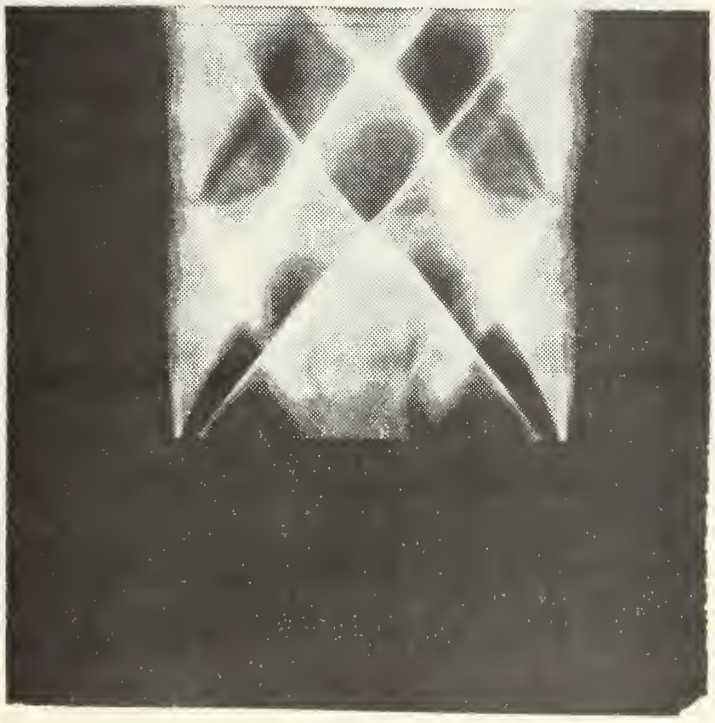

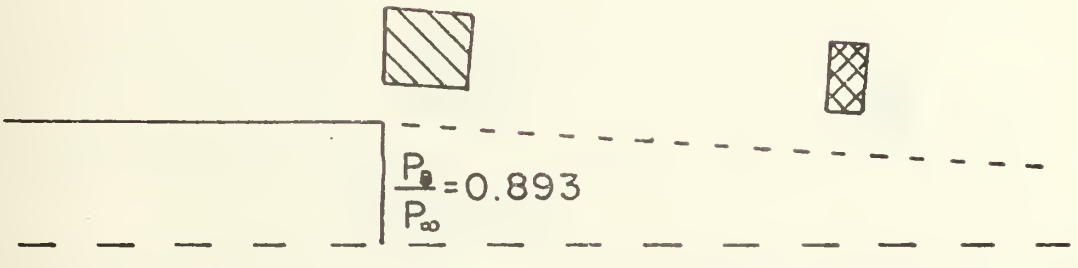

FIG. 38

PHOTOGRAPH AND SCHEMATIC FOR $W/h = 0.72$, $\ell/h = 0.0$

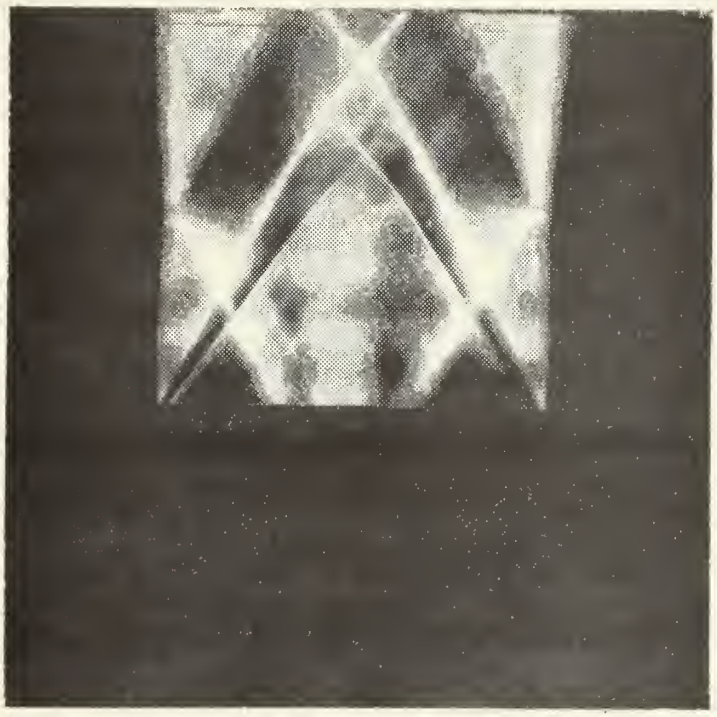

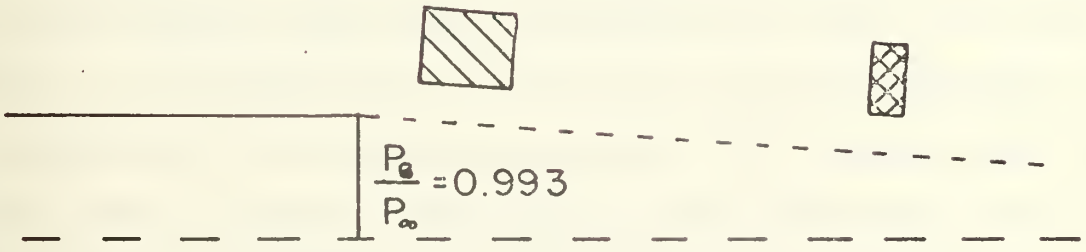

FIG. 39
PHOTOGRAPH AND SCHEMATIC FOR W/h =0.72, ℓ/h =0.50

A study of the pictures shows that a uniformly distributed heat source was not obtained as desired. Instead, the starting compression waves, which originated immediately downstream of the nozzle throat, reflected from the cylinder wall to the nozzle corner and then into the base flow region as shownat the top of Figs. 40, 41, and 42. For the W/h = 4.34 nozzle, the simulated heating distribution is shown in the middle of Fig. 40.

Compression, originating from the simulated heat addition zone, starts at point b and increases to uniform strength at point e where it levels at a constant value until just prior to point h. The reflected compression waves from the nozzle corner superimposed upon the uniform heat cause a spike which is approximately twice the magnitude of the intended uniform value. This spike is seen in the W/h = 4.34 photographs as a shock wave, formed by a coalescing of the reflected compression waves, as seen in Figs. 25-29.

Figures 41 and 42 show the expected compression wave reflection pattern and heat distribution for W/h = 1.84 and W/h = 0.72 respectively. Basically, the same phenomena of compression wave reflection occurred. The shorter heat addition zones, however, ended prior to the reflection, and, therefore, the reflected waves created an almost equal strength combustion region downstream of the intended heat addition zone rather than a spike as seen for the W/h = 4.34 case.

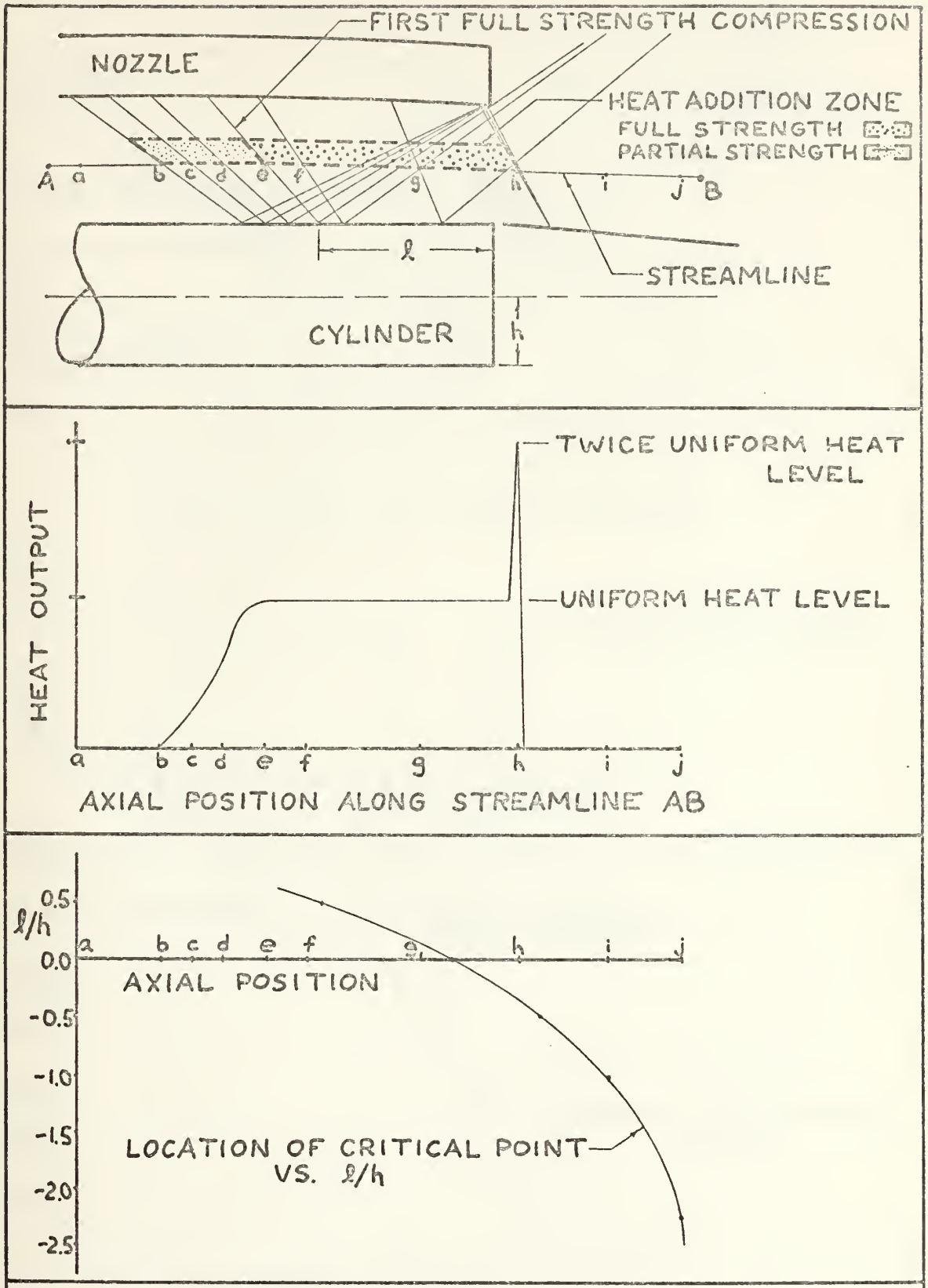

FIG. 40
COMPRESSION WAVE BEHAVIOR, HEAT DISTRIBUTION AND CRITICAL POINT LOCATION FOR W/h=4.34 NOZZLE

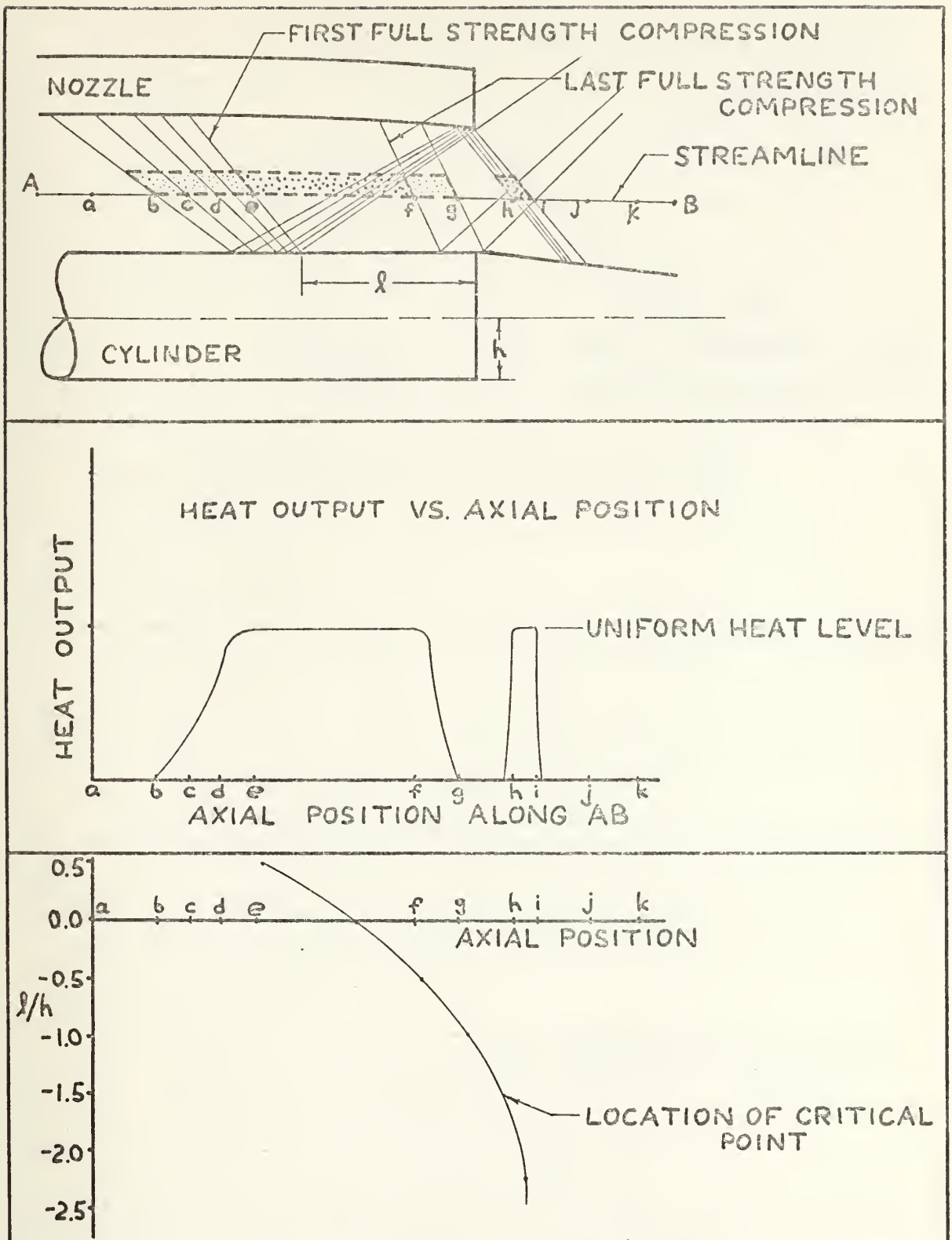

FIG. 41
COMPRESSION WAVE BEHAVIOR, HEAT DISTRIBUTION, AND CRITICAL POINT LOCATION FOR W/h=1.84 NOZZLE

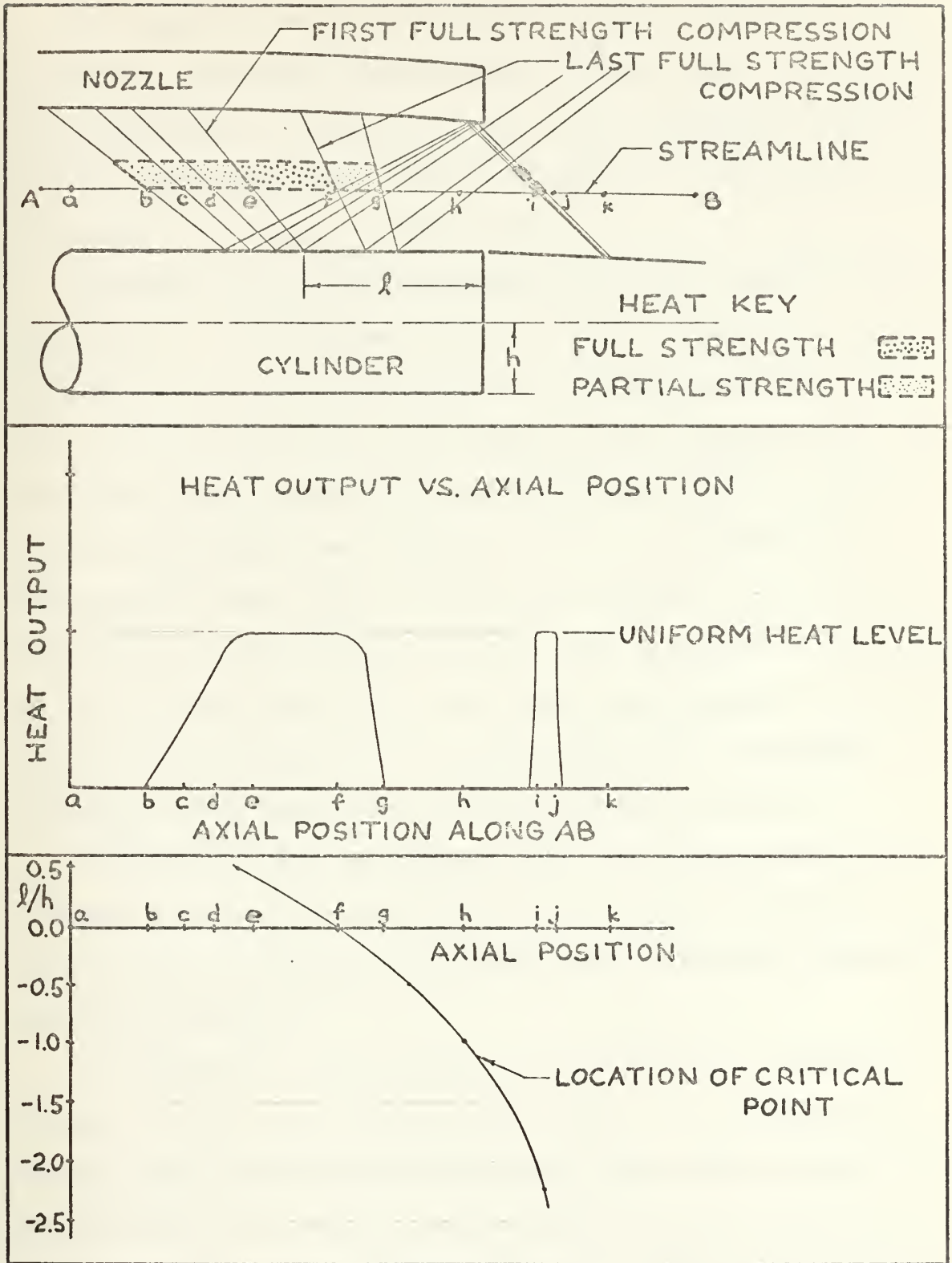

FIG. 42

COMPRESSION WAVE BEHAVIOR, HEAT DISTRIBUTION AND CRITICAL POINT LOCATION FOR W/h = 0.72 NOZZLE

The photographs show that for the W/h = 1.84 case, the reflected compression waves never coalesce into a shock but are spread over a slightly longer axial distance. For W/h = 0.72, a shock did form, but its strength is notably less than the shock occurring for W/h = 4.34.

Although the reflected compression waves existed for each data point, it is assumed that the base pressure was affected by the reflection for only the points circled in Fig. 24. The circled points were determined by the location where the reflected wave impinged the recirculation bubble. As previously described, base pressure can be influenced by compression waves only if the waves interact with the base flow prior to the critical point. Any interaction downstream of the critical point will not influence pressure at the base. The bottom of Figs. 40, 41, and 42 shows the estimated critical point location for the three W/h nozzles.

A vertical line extended through the intersection of a given l/h value and the critical point curve will have on its left the portion of the heat addition region affecting the base pressure.

In conclusion, it is evident that external burning is capable of not only reducing base drag but also producing thrust under the proper conditions. The optimal benefit is derived when the entire recirculation bubble is embedded in combustion created compression waves. Waves beginning upstream of the base corner have limited value for raising base pressure, and waves interacting downstream of the critical point are wasted.

LIST OF REFERENCES

1. Chapman, D. R., "An Analysis of Base Pressure at Supersonic Velocities and Comparison with Experiment", NACA TN 2137, July 1950.

2. Crocco, L. and Lees, L., "A Mixing Theory for the Interaction Between Dissipative Flows and Nearly Isentropic Streams", Journal of Aeronautical Sciences, Vol. 19, No. 10, October 1952.

3. Darling, J. A. and Knott., J., "Effect of Spin on the Aerodynamics of the 20mm Projectile", Naval Ordnance Laboratory, TR 71-180, September 1971.

4. Davis, Dale D., "Extension of Simplified Mixing Theory to Axially Symmetric Supersonic Wake Flows and Application to the Base Pressure Problem for a Body of Revolution", Princeton University Master of Science Thesis 24-V-1952.

5. Dickinson, Elizabeth R., "Some Aerodynamic Effects of Varying Body Length of a Spinning Projectile", Ballistic Research Laboratories, MR 1664, July 1965.

6. Fuhs, A. E., "Quasi Area Rule for Heat Addition in Transonic and Supersonic Flight Regime", AFAPL-TR-72-10, August 1972.

7. Fuhs, A. E., Smithey, W., and Naber, M., "Axisymmetric Analysis of External Burning Assisted Projectile", 9th JANNAF Combustion Meeting, CPIA Publication 231, Vol. II, December 1972, pp. 389-416.

8. Kurzweg, H. H., "Interrelationship Between Boundary Layer and Base Pressure", Journal of the Aeronautical Sciences, Vol. 18, No. 11, November 1931.

9. Lehnert R., and Hastings, S. M., "Spin Effects on Base Pressure of Cone Cylinders at M = 2.86", Naval Ordnance Laboratory, TR 2956, October 1953.

10. Przirembel, G. E., and Page, R. H., "Analysis of Axisymmetric Supersonic Turbulent Base Flow", Heat Transfer and Fluid Mechanics Institute Proceedings, pp. 258-272, 1968.

11. Schmidt, L. E., and Murphy, C. H., "Effect of Spin on Aerodynamic Properties of Bodies of Revolution", Ballistic Research Laboratories Report 715, November 1953.

12. Sedney, R., "Review of Base Drag", U. S. Army Ballistic Research Laboratories Report 1337, October 1966.

13. Strahle, W. C., "Theoretical Consideration of Combustion Effects on Base Pressure in Supersonic Flight", Twelfth Symposium on Combustion, Combustion Institute, Pittsburgh, Pennsylvania, 1969.

INITIAL DISTRIBUTION LIST

		No. of Copies
1.	Defense Documentation Center Cameron Station Alexandria, Virginia 22314	2
2.	Library, Code 0212 Naval Postgraduate School Monterey, California 93940	2
3.	Professor A. E. Fuhs Department of Aeronautics Naval Postgraduate School Monterey, California 93940	5
4.	Ltjg. Gary J. Caswell, USN 399 Troy Aurora, Colorado 80010	3
5.	Dr. Warren Strahle Aerospace Engineering Georgia Institute of Technology Atlanta, Georgia 30332	1
6.	Mr. Dominic J. Monetta Gun Systems Engineering Naval Ordnance Station Indian Head, Maryland 20640	2
7.	Dr. Alan Roberts Gun Systems Engineering Naval Ordnance Station Indian Head, Maryland 20640	2
8.	Dr. Frederick Billig Applied Physics Laboratory Johns Hopkins University 8621 Georgia Avenue Silver Springs, Maryland 20910	1
9.	Professor Bruce Reese Chairman of Aeronautical Engineering Purdue University Lafayette, Indiana 47907	1
10.	Cmdr. William Smithey SMC, Box 2348 Naval Postgraduate School Monterey, California 93940	3

11. Dr. James S. Holdhusen — 1
Vice President
FluiDyne Engineering Corporation
5900 Olsen Highway
Minneapolis, Minnesota 55422

12. Mr. Thomas Curran — 1
Chief of Ramjet Technology Branch
Air Force Applied Physics Laboratory
Wright Patterson Air Force Base, Ohio 45433

13. Lt. Noel P. Horn, USN — 1
SMC, Box 1183
Naval Postgraduate School
Monterey, California 93940

14. Dr. Grant Hosack — 1
Rocketdyne
Rockwell International
6633 Canoga Avenue
Canoga Park, California 91304

15. Mr. C. Miner — 1
U. S. Army Missle Command
Redstone Arsenal, Alabama

16. Dr. Richard Weiss — 1
Air Force Rocket Propulsion Laboratory
Edwards Air Force Base, California

17. Professor John Clarke — 1
Cranfield Institute of Technology
Bedford, England

18. Dr. E. G. Broadbent — 1
Royal Aeronautical Establishment
Farnborough, England

19. Chairman, Department of Aeronautics — 2
Naval Postgraduate School
Monterey, California 93940

20. Dr. Ing. G. Winterfeld — 1
D F V L R
Institut f. Luftstrahlantriebe
505 Porz-Wahn, Linder Höhe, Germany

SECURITY CLASSIFICATION OF THIS PAGE (When Data Entered)

REPORT DOCUMENTATION PAGE		READ INSTRUCTIONS BEFORE COMPLETING FORM
1. REPORT NUMBER	2. GOVT ACCESSION NO.	3. RECIPIENT'S CATALOG NUMBER
4. TITLE (and Subtitle) Base Drag Reduction by External Burning		5. TYPE OF REPORT & PERIOD COVERED Master's Thesis September 1973 6. PERFORMING ORG. REPORT NUMBER
7. AUTHOR(s) Gary Joe Caswell		8. CONTRACT OR GRANT NUMBER(s)
9. PERFORMING ORGANIZATION NAME AND ADDRESS Naval Postgraduate School Monterey, California 93940		10. PROGRAM ELEMENT, PROJECT, TASK AREA & WORK UNIT NUMBERS
11. CONTROLLING OFFICE NAME AND ADDRESS Naval Postgraduate School Monterey, California 93940		12. REPORT DATE September 1973 13. NUMBER OF PAGES 77
14. MONITORING AGENCY NAME & ADDRESS(if different from Controlling Office) Naval Postgraduate School Monterey, California 93940		15. SECURITY CLASS. (of this report) Unclassified 15a. DECLASSIFICATION/DOWNGRADING SCHEDULE

16. DISTRIBUTION STATEMENT (of this Report)

Approved for public release; distribution unlimited.

17. DISTRIBUTION STATEMENT (of the abstract entered in Block 20, if different from Report)

18. SUPPLEMENTARY NOTES

19. KEY WORDS (Continue on reverse side if necessary and identify by block number)

Base Drag Reduction
Axisymmetric Heat Addition
Spin Effects on Base Pressure

20. ABSTRACT (Continue on reverse side if necessary and identify by block number)

Supersonic combustion in the inviscid stream has been shown to reduce the base drag on a projectile. Fast reacting fuel burned externally in the inviscid, supersonic flow generates compression waves, which, when properly originated, impinge on the recirculation bubble aft of the projectile base and increase the base pressure. A free-jet wind tunnel was constructed to study external burning where heat addition was simulated by

DD FORM 1 JAN 73 1473 EDITION OF 1 NOV 65 IS OBSOLETE
S/N 0102-014-6601 |
(Page 1)

SECURITY CLASSIFICATION OF THIS PAGE (When Data Entered)

20. ABSTRACT (Continued)

nozzle contour. Sufficient increase in base pressure was attained to not only reduce base drag but also provide thrust. Thus, external burning provides a method for increasing the performance of projectiles.

146323
Thesis
C3255 Caswell
c.1 Base drag reduction
by external burning.